Deliverable Report

Deliverable No: D2.6

Deliverable Title: Polarization-OAM qudits

Grant Agreement number: 255914

Project acronym: PHORBITECH

Project title: A Toolbox for Photon Orbital Angular Momentum Technology

Project website address: www.phorbitech.eu

Name, title and organisation of the scientific representative of deliverable's lead beneficiary (task leader):

Dr. Fabio Sciarrino
Sapienza Università di Roma (UROM)
Roma, Italy

Deliverable table

Deliverable no.	D2.6
Deliverable name	Polarization-OAM qudits
WP no.	2
Lead beneficiary no.	2 (UROM)
Nature	R
Dissemination level	PU
Delivery date from Annex I	Month 24
Actual delivery date	30 September 2012

D2.6) Polarization-OAM qudits: Generation / manipulation of polarization-OAM qudits with dimension larger than 4, obtained by coherently superimposing different OAM subspaces and the polarization space. In connection with this, the optimal strategies to efficiently reconstruct the quantum states of Hilbert space with increasing size will be also investigated.
[*Excerpt from the Annex describing the deliverables of WP2, page 16*]

The generation of qudit quantum states can open new prospects both for fundamental test of quantum mechanics and for the implementation of quantum improved tasks. The second year of the project has been mainly focused on fully exploiting the potentialities of four-dimensional quantum systems for fundamental and technological applications. This work has been performed by UROM, but ICFO has also started working on this goal with success. The implementation of even larger dimensionality, carried out by UROM in collaboration with UNAP, is currently under way.

Four publications (3 in journals, 1 posted in arXiv and submitted) are included in this deliverable.

In [1] UROM, in collaboration with the University of Sevilla, has introduced an innovative cryptographic scheme. Quantum cryptographic protocols based on complementarity are not secure against attacks in which complementarity is imitated with classical resources. The Kochen-Specker (KS) theorem provides protection against these attacks, without requiring entanglement or spatially separated composite systems. UROM analyzed the maximum tolerated noise to guarantee the security of a KS-protected cryptographic scheme against these attacks and described a photonic realization of this scheme using hybrid ququarts defined by the polarization and orbital angular momentum of single photons

In [2] UROM, in collaboration with the University of Sevilla, has exploited ququart states to perform tests of quantum mechanics. Quantum resources outperform classical ones for certain communication and computational tasks. Remarkably, in some cases, the quantum advantage cannot be improved using hypothetical postquantum resources. A class of tasks with this property can be singled out using graph theory. UROM reported the experimental observation of an impossible-to-beat quantum advantage on a four-dimensional quantum system defined by the polarization and orbital angular momentum of a single photon. The results show pristine evidence of the quantum advantage and are compatible with the maximum advantage allowed using postquantum resources.

In [3], UROM in collaboration with the University of Sevilla and Stockholm has implemented the first Kochen-Specker set of quantum tests. Kochen-Specker (KS) sets are collections of yes-no tests for which results cannot be preassigned in agreement with the predictions of quantum mechanics for any arbitrary quantum state of a given quantum system of dimension three or higher. KS sets have both fundamental and practical importance, can be used for tasks which cannot be performed with classical resources, and have the distinguishing feature that the quantum advantage is free of the initialization problem of quantum computing. In addition, some KS sets provide a quantum advantage which cannot be outperformed by any post-quantum resources. We reported the first experimental implementation of a complete KS set and show how to use it to obtain state-independent impossible-to-beat quantum advantages. UROM demonstrated the unique power of a 4-dimensional 18-test KS set for solving a specific task avoiding the problem of state initialization and reaching the maximum performance, by demonstrating that, for 28 different quantum states encoded in the orbital angular momentum and path degrees of freedom of single photons, the KS set provides an impossible-to-beat solution to this task. In a second experiment,

the University of Stockholm generated state-independent fully contextual quantum correlations by performing compatible sequential measurements of the polarization and path of single photons, exploiting the fact that these sequences project any initial quantum state into one of the eigenstates of the KS set.

In [4], in advance with respect to the plans, ICFO has successfully carried out a test on dimensional witness adopting OAM quantum states. An overwhelming majority of experiments in classical and quantum physics make a priori assumptions about the dimension of the system under consideration. However, would it be possible to assess the dimension of a completely unknown system only from the results of measurements performed on it, without any extra assumption? The concept of a dimension witness answers this question, as it allows one to bound the dimension of an unknown classical or quantum system in a device-independent manner, that is, only from the statistics of measurements performed on it. ICFO reported on the experimental demonstration of dimension witnesses in a prepare and measure scenario. ICFO used pairs of photons entangled in both polarization and orbital angular momentum to generate ensembles of classical and quantum states of dimensions up to four. These results open new avenues for the device-independent estimation of unknown quantum systems and for applications in quantum information science. The result here reported is relevant both for this deliverable and for deliverable D2.10, on quantum information tasks in the OAM-polarization space.

UROM and UNAP are currently working jointly on the implementation of hybrid qusix states based on polarization and OAM encoding. The first preliminary results have been already obtained and the experiment should be completed within month 27 and will therefore be included in deliverable D2.10.

PHORBITECH contribution to this deliverable

PHORBITECH has supported the entire cost of the post-doc personnel (Eleonora Nagali, Ebrahim Karimi) and part of the cost of the PhD students (Vincenzo D'Ambrosio) and the staff personnel. Moreover, PHORBITECH, jointly with the FIRB project HYTEQ (Italian Ministry for Research), has also supported the purchase of the needed equipment and lab materials. All quantum optics experiments have been performed in UROM, with PHORBITECH involved people. Adan Cabello, from the University of Sevilla, has contributed to papers [1]-[3] for the theory on quantum contextuality. In [3] the group of Mohammed Bourennane, from the University of Sevilla, has carried out part of the experiments with an experimental approach based on polarization-path encoding that complemented the experiments carried out in Rome.

PHORBITECH contributors to this deliverable:

UROM: Eleonora Nagali, Vincenzo D'Ambrosio, Sandro Giacomini, Giorgio Milani, Fabio Sciarrino
UNAP: Ebrahim Karimi, Enrico Santamato, Lorenzo Marrucci
ICFO: Martin Hendrych, Michal Micuda, Juan P. Torres

Publications included in this deliverable:

[1] “Hybrid ququart-encoded quantum cryptography protected by Kochen-Specker contextuality”, A. Cabello, V. D'Ambrosio, E. Nagali, F. Sciarrino, *Physical Review A* **84**, 030302 (2011).

[2] “Experimental observation of impossible-to-beat quantum advantage on a hybrid photonic system”, E. Nagali, V. D’Ambrosio, F. Sciarrino, A. Cabello, *Physical Review Letters* **108**, 090501 (2012)

[3] “Experimental implementation of a Kochen-Specker set of quantum tests”, V. D’Ambrosio, I. Herbauts, E. Amselem, E. Nagali, M. Bourennane, F. Sciarrino, and A. Cabello, paper submitted, published online at arXiv:1209.1836.

[4] “Experimental estimation of the dimension of classical and quantum systems”, M. Hendrych, R. Gallego, M. Micuda, N. Brunner, A. Acín, J.P. Torres, *Nature Physics* **8**, 588-591 (2012). DOI: 10.1038/nphys2334. [NOTE: this publication will be also reported at month 36 as part of deliverable D2.10]

PHYSICAL REVIEW A **84**, 030302(R) (2011)

Hybrid ququart-encoded quantum cryptography protected by Kochen-Specker contextuality

Adán Cabello,[1,2,*] Vincenzo D'Ambrosio,[3] Eleonora Nagali,[3] and Fabio Sciarrino[3,4,†]
[1]*Departamento de Física Aplicada II, Universidad de Sevilla, E-41012 Sevilla, Spain*
[2]*Department of Physics, Stockholm University, S-10691 Stockholm, Sweden*
[3]*Dipartimento di Fisica della "Sapienza" Università di Roma, I-00185 Roma, Italy*
[4]*Istituto Nazionale di Ottica, Consiglio Nazionale delle Ricerche (INO-CNR), I-50125 Florence, Italy*
(Received 22 July 2011; published 12 September 2011)

Quantum cryptographic protocols based on complementarity are not secure against attacks in which complementarity is imitated with classical resources. The Kochen-Specker (KS) theorem provides protection against these attacks, without requiring entanglement or spatially separated composite systems. We analyze the maximum tolerated noise to guarantee the security of a KS-protected cryptographic scheme against these attacks and describe a photonic realization of this scheme using hybrid ququarts defined by the polarization and orbital angular momentum of single photons.

DOI: 10.1103/PhysRevA.84.030302 PACS number(s): 03.67.Dd, 03.65.Ud, 42.50.Xa, 42.50.Tx

Introduction. Quantum key distribution (QKD) protocols allow two distant parties to share a secret key by exploiting the fundamental laws of quantum mechanics. However, standard quantum cryptographic protocols based on quantum complementarity, such as the Bennett-Brassard 1984 (BB84) protocol [1], are not secure against attacks in which the adversary imitates complementarity with classical resources [2]. Interestingly, BB84-like protocols can be improved to assure "the best possible protection quantum theory can afford" [2] by exploiting the fact that the Bell [3] and Kochen-Specker (KS) [4] theorems show that the outcomes of quantum measurements do not admit local and noncontextual descriptions, respectively. The extra security provided by the Bell theorem has been extensively investigated [5–7]. However, this extra security is based on the assumption that the legitimate parties can perform a loophole-free Bell test, something which is beyond the present technological capabilities and is not expected to be an easy task in the future [8]. A similar problem affects recent proposals combining the KS theorem with entanglement [9,10]. Therefore, it is worth exploring the extra security offered by the KS theorem in situations which require neither entanglement nor composite systems, but only single systems with three or more distinguishable states. For cryptographic purposes, the difference between qubits and systems of higher dimensionality is this: Whereas in qubits different bases are always disjoint, from qutrits onward different bases may share common elements. It is this property which is at the root of the proofs of Bell and KS theorems.

Here we investigate the experimental requirements for obtaining the extra security offered by a KS-protected QKD protocol introduced by Svozil [11], based on the properties of the simplest KS set of states [12]. Hence we propose to implement such a protocol by adopting ququart states encoded in the hybrid polarization-orbital angular momentum four-dimensional space of single photon states [13,14]. For this purpose, we introduce the optical schemes to measure all the states needed to prove KS contextuality. The capability of encoding a four-dimensional quantum state in a single photon by exploiting these two different degrees of freedom enables us to achieve a high stability and transmission rate in free-space propagation.

Svozil's protocol. The cryptographic protocol introduced by Svozil in [11] is a variation of the BB84 protocol and works as follows: (i) Alice randomly picks a basis from the nine available in Fig. 1 and sends Bob a randomly chosen state of that basis. (ii) Bob, independently from Alice, picks a basis at random from the nine available and measures the system received from Alice. (iii) Bob announces his bases over a public channel, and Alice announces those events in which the state sent belongs to the measured basis. Therefore, the probability of adopting the same basis is $\frac{1}{9}$. (iv) Alice and Bob exchange some of the remaining matching outcomes over a public channel to ensure that nobody has spied their quantum channel. (v) Alice and Bob encode the four outcomes by using four different symbols. As a result, for each successful exchange Bob and Alice share a common random key.

The advantage of this protocol over the BB84 protocol is that it is protected by the KS theorem against attacks in which the adversary replaces the quantum system with a classical one. These attacks can be described using a classical toy model [2,11] in which, in step (i), Alice is actually picking one of nine differently colored eyeglasses (instead of one of the nine different bases in Fig. 1) and picking a ball from an urn (instead of picking one of the 18 states in Fig. 1) with two color symbols in it (corresponding to the two bases the state belongs to). Each one of the nine differently colored eyeglasses allows her to see only one of the nine different colors. To reproduce the quantum predictions: (a) each of the balls must have one symbol $S_i \in \{1,2,3,4\}$ written in two different colors chosen among the 18 possible pairs. Her choice of eyeglass decides which symbols Alice can see. (b) All colors are equally probable and, for a given color, the four symbols are equally probable. In step (ii), Bob is actually picking one of nine differently colored eyeglasses and reading the corresponding symbol. A classical strategy like this one can successfully imitate the quantum part of the BB84 protocol (see [2] for details) but not the protocol described above. The reason is that the requirements (a) and (b) cannot be satisfied simultaneously. Figure 1 shows how to

*adan@us.es
†fabio.sciarrino@uniroma1.it http://quantumoptics.phys.uniroma1.it

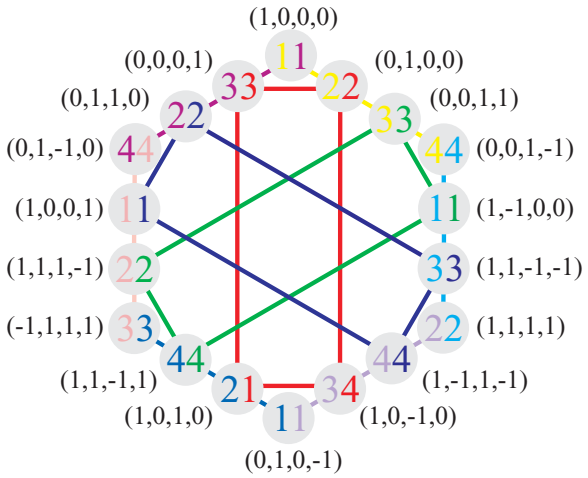

FIG. 1. (Color online) The protocol is based on a KS set of 18 states which can be grouped in 9 bases represented by 9 colors. Every state belongs to two different bases. No set of 18 balls can have all the properties required to imitate the KS set; at least two balls must have different symbols. Therefore, the imitation can be detected.

prepare 18 balls with the minimum number of balls not having the same symbol.

Experimental requirements. As shown in Fig. 1, the minimum number of balls not having the same symbol is two out of 18. A ball attack can be detected only in those runs in which Alice and Bob pick differently colored eyeglasses. Therefore, for the set in Fig. 1, the trace of such an attack will be a $\frac{2}{18}$ probability of Alice picking a symbol such that the corresponding interlinked symbol (seen only with differently colored eyeglasses) is different. As a consequence, to demonstrate that the experimental results cannot actually be imitated with balls and to experimentally certify the extra security of this KS-based QKD protocol, we need an experimental probability w of wrong state identification, defined as the probability that Bob makes a wrong identification of the state sent by Alice when Bob has successfully measured in a correct basis, of $w < \frac{1}{9} \approx 0.111$.

Implementation using polarization- and orbital-angular-momentum-encoded ququarts. Here we propose a scheme for the experimental implementation of the KS-protected QKD protocol. To test its feasibility, we need to prepare the 18 states, measure each of them in two different bases, and obtain an average value of w over the 18×2 possibilities. The condition which must be fulfilled is $w < 0.111$, which corresponds to a mean fidelity value of the transmission of the state of $F = 0.889$. In addition, to check that any intercept and resend strategy causes a disturbance, one should be able to measure what happens when the states are measured in the wrong basis. While in the correct basis the probabilities for the four possible outcomes are (in the ideal case) 0, 0, 0, and 1, in the wrong basis they are either 0, 0, $\frac{1}{2}$, and $\frac{1}{2}$ or 0, $\frac{1}{4}$, $\frac{1}{4}$, and $\frac{1}{2}$.

Svozil's protocol uses nine sets of four-dimensional states defining a 18-state KS set. We propose encoding four-dimensional quantum states by exploiting two different degrees of freedom of the same particle, an approach that allows us to achieve higher efficiency in the transmission process. It has recently been demonstrated that ququart states can be efficiently generated by manipulating the polarization and orbital angular momentum (OAM) of a single photon [13]. In particular, we consider a bidimensional subset of the infinite-dimensional OAM space, denoted as o_1, spanned by states with OAM eigenvalue $m = \pm 1$ in units of $\hbar$. According to the nomenclature $|\varphi,\phi\rangle = |\varphi\rangle_\pi |\phi\rangle_{o_1}$, where $|\cdot\rangle_\pi$ and $|\cdot\rangle_{o_1}$ stand for the photon quantum state "kets" in the polarization and OAM degrees of freedom, the logic ququart basis can be rewritten as

$$\{|1\rangle,|2\rangle,|3\rangle,|4\rangle\} \rightarrow \{|H,+1\rangle,|H,-1\rangle,|V,+1\rangle,|V,-1\rangle\}, \quad (1)$$

where H (V) refers to horizontal (vertical) polarization. Following the same convention, the OAM equivalent of the basis $|H\rangle$ and $|V\rangle$ is then defined as $|h\rangle = \frac{1}{\sqrt{2}}(|+1\rangle + |-1\rangle)$ and $|v\rangle = \frac{i}{\sqrt{2}}(|+1\rangle - |-1\rangle)$. Finally, the $\pm 45^\circ$ angle "antidiagonal" and "diagonal" linear polarizations are hereafter denoted by the kets $|A\rangle = (|H\rangle + |V\rangle)/\sqrt{2}$ and $|D\rangle = (|H\rangle - |V\rangle)/\sqrt{2}$, while the OAM equivalent is denoted by $|a\rangle = (|h\rangle + |v\rangle)/\sqrt{2}$ and $|d\rangle = (|h\rangle - |v\rangle)/\sqrt{2}$. It is convenient to work with Laguerre-Gauss laser modes ($LG_{0,\pm 1}$) as OAM eigenstates since, in this case, the states ($|h\rangle$,$|v\rangle$,$|a\rangle$,$|d\rangle$) will result as the Hermite-Gauss modes ($HG_{1,0}$,$HG_{0,1}$) along the axes and rotated by 45°. This feature allows us to easily transform the states by an astigmatic laser mode converter [15]. We stress that by choosing a bidimensional subspace of OAM we avoid detrimental effects on the state due to the radial contribution in the free propagation and Gouy-phases associated with different OAM values [16]. Hence, a hybrid approach for the encoding of a ququart state, based on OAM and polarization, leads to a higher stability for the single photon propagation compared to a qudit implemented only by adopting the OAM degree of freedom. According to the previous definitions, a state (a_1,a_2,a_3,a_4) of the KS set is implemented as

$$a_1|H,+1\rangle + a_2|H,-1\rangle + a_3|V,+1\rangle + a_4|V,-1\rangle. \quad (2)$$

The coefficients a_i for each state are shown in Table I, along with the settings needed to analyze each basis.

Generation. Figure 2 shows the optical schemes for the generation and detection of any ququart state of the KS set. The generation of the states can be achieved by adopting a spontaneous parametric down conversion (SPDC) source of pair of photons, as in Fig. 2(a), where we consider a collinear generation of couples $|H\rangle|V\rangle$, where one of the two photons acts as a trigger for the heralded generation of a single photon to be sent to the experimental setup. As in [13], the manipulation of the OAM degree of freedom can be achieved by adopting the q-plate device [16,17]. On the polarization, the q plate acts as a half-wave plate, while on the OAM it imposes a shift on the eigenvalue $m = \pm 2q$, where q is an integer or half-integer number determined by the (fixed) pattern of the optical axis of the device. In order to manipulate the OAM subspace $o_1 = \{|+1\rangle,|-1\rangle\}$, a q plate with topological charge $q = 1/2$ should be adopted [18]. Interestingly, the fact that the q plate can entangle or disentangle the OAM and polarization degrees of freedom can be exploited for the preparation of any ququart states. In order to generate all the states of the KS set, it is sufficient to exploit a technique based on a quantum transferrer

TABLE I. The ququart states that compose the KS set are divided in nine basis and encoded in polarization and orbital angular momentum degrees of freedom by adopting the devices in Fig. 2. Column E identifies whether or not the states are entangled states of the two degrees of freedom. Column S specifies the experimental setup to be adopted for the analysis. Column MC gives the angle between the horizontal axis and the orientation of the cylindrical lenses of the mode converter MC. Column QWP indicates the angle of the quarter wave plate to be inserted after the PSI in Fig. 2(b) for the analysis of bases IV and IX.WP refers to the type of wave plate to be inserted in the setup: H means half-wave plate and Q means quarter-wave plate.

Set	Logic	E	S	PSI1	PSI2	QWP	MC	WP
I	(1,0,0,0),(0,1,0,0)		b				$\frac{\pi}{4}$	
	(0,0,1,1),(0,0,1, − 1)		b				$\frac{\pi}{4}$	
II	(1,1,1,1),(1,1, − 1, − 1)		c				$\frac{\pi}{4}$	H $\frac{\pi}{8}$
	(1, − 1,0,0),(0,0,1, − 1)		c				$\frac{\pi}{4}$	H $\frac{\pi}{8}$
III	(1,1,1,1),(1, − 1,1, − 1)		b				$\frac{\pi}{4}$	
	(1,0, − 1,0),(0,1,0, − 1)		b				$\frac{\pi}{4}$	
IV	(−1,1,1,1),(1,1, − 1,1)	✓	b	✓		$\frac{\pi}{4}$	0	
	(1,0,1,0),(0,1,0, − 1)		b	✓		$\frac{\pi}{4}$	0	
V	(1,0,0,1),(0,1, − 1,0)	✓	c	✓	✓		$\frac{\pi}{4}$	H $\frac{\pi}{8}$
	(1,1,1, − 1),(−1,1,1,1)	✓	c	✓	✓		$\frac{\pi}{4}$	H $\frac{\pi}{8}$
VI	(1,0,0,1),(0,1,1,0)	✓	c		✓		0	Q $\frac{\pi}{4}$
	(1,1, − 1, − 1),(1, − 1,1, − 1)		c		✓		0	Q $\frac{\pi}{4}$
VII	(1,1,1, − 1),(1,1, − 1,1)	✓	c		✓		0	Q $\frac{\pi}{4}$
	(0,0,1,1),(1, − 1,0,0)		c		✓		0	Q $\frac{\pi}{4}$
VIII	(0,0,0,1),(1,0,1,0)		c					H $\frac{\pi}{8}$
	(1,0, − 1,0),(0,1,0,0)		c					H $\frac{\pi}{8}$
IX	(0,1, − 1,0),(0,1,1,0)	✓	b	✓		$\frac{\pi}{4}$	0	
	(1,0,0,0),(0,0,0,1)		b	✓		$\frac{\pi}{4}$	0	

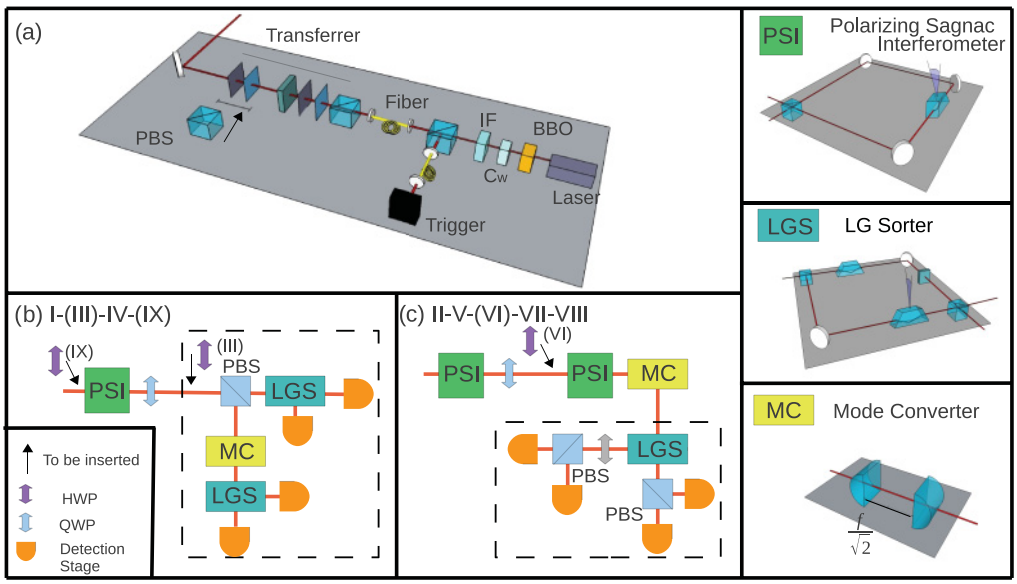

FIG. 2. (Color online) (a) Setup for the generation of ququart states: One of the two photons emitted by SPDC acts as a trigger, while the other one is sent to a polarizing beam splitter (PBS), wave plates, and a quantum transferrer based on the q plate in order to generate the desired ququart. (b) Setup for the analysis of bases (I-III-IV-IX): The setup in the dotted rectangle analyzes the four states of basis I; basis III can be measured by inserting a half-wave plate (HWP) at $\pi/8$ before the PBS. A polarizing Sagnac interferometer (PSI) and a quarter-wave plate are needed to analyze bases IV and IX (adding a HWP at $\pi/8$ before the PSI). (c) Setup for the analysis of bases (II-V-VI-VII-VIII): The part in the dotted rectangle is suitable to sort the four states of all the bases (the gray wave plate can be a HWP or a QWP depending on the particular basis as shown in Table I); this part is sufficient to analyze basis VIII. Basis II can be analyzed by adding a mode converter (MC). Using a PSI before the MC makes it possible to analyze bases VI (adding a HWP at $\pi/8$) and VII. Finally, the states of basis V can be sorted by an additional PSI and QWP. The pictures in the three boxes on the right represent the Sagnac interferometer, the LG mode sorter, and the cylindrical lens mode converter, respectively. The detection stage consists of a q plate, a single-mode fiber, and a detector.

$\pi \rightarrow o_1$ described in [13]. The OAM eigenmodes produced in this way are not exactly LG modes but hypergeometric Gaussian ones [19]. Since some of the detection schemes are based on the properties of Laguerre-Gaussian modes, this fact will lead, in some cases, to a detection efficiency of around 80%. Thus, in order to avoid noise due to different OAM order contributions, it is sufficient to insert in the detection stage a q plate and a single-mode fiber connected to the detector (see Fig. 2).

Measurement of the KS bases. The bases involved in the KS set have different structures as shown in Table I. They can be classified in three groups, depending on whether they are composed of separable, entangled (between polarization and OAM), or both separable and entangled states.

The detection setup is shown in Figs. 2(b) and (c). Their components are a polarizing Sagnac interferometer with a Dove prism (PSI) [20], an astigmatic laser mode converter (MC) [15], and a Laguerre-Gauss mode sorter (LGS) [21]. The PSI consists of a Sagnac interferometer with a polarizing beam splitter as input-output gate and a Dove prism that intercepts the two counterpropagating beams and can be rotated around the optical axes. This scheme allows us, under appropriate conditions, to transform an entangled state into a separable one. In this case, the prism must be rotated in order to add a phase shift of $\Delta\phi = \pi/2$ between $|H\rangle$ and $|V\rangle$ ($\alpha = \pi/8$ in Fig. 2). For example, the states of basis IV are transformed into $(|L,a\rangle,|L,d\rangle,|R,+1\rangle,|R,-1\rangle)$. The MC consists of two cylindrical lenses (with the same focal length f) at distance $f/\sqrt{2}$. It allows us to convert the HG states $(|a\rangle,|d\rangle)$ into $(|+1\rangle,|-1\rangle)$ and, if rotated by 45° along the optical axes, to convert $(|h\rangle, |v\rangle)$ into $(|+1\rangle, |-1\rangle)$ [15]. The LGS consists of a Mach-Zehnder interferometer with a Dove prism in each arm. The two prisms are rotated by $\beta = \pi/4$ with respect to each other. A phase plate ($\psi = \pi/2$) in one of the two arms allows us to send $|+1\rangle$ and $|-1\rangle$ in the two different output ports of the Mach-Zehnder. States belonging to sets I-III-IV-IX can be analyzed by adopting the scheme reported in Fig. 2(b) with some slight modifications related to the specific basis to be measured. The scheme in Fig. 2(c) leads to the analysis of bases II-V-VI-VII-VIII. All the details on the settings of the different measurement devices are in Table I.

Conclusions. Device-independent QKD based on loophole-free Bell tests are still far in the future. It is therefore worth investigating whether quantum contextuality can produce some extra protection to BB84-like protocols which do not use entangled states. Here we have presented a proposal to demonstrate a quantum contextuality-based extra protection against a particular attack, requiring neither composite systems nor entangled states.

Acknowledgments. We acknowledge helpful discussions with E. Karimi and L. Marrucci. This work was supported by the MICINN Project No. FIS2005-07689, the Wenner-Gren Foundation, FIRB Futuro in Ricerca-HYTEQ, and Project PHORBITECH of the Future and Emerging Technologies (FET) program within the Seventh Framework Programme for Research of the European Commission, under FET-Open Grant No. 255914.

[1] C. H. Bennett and G. Brassard, in *Proceedings of IEEE International Conference on Computers, Systems, and Signal Processing, Bangalore, India* (IEEE, New York, 1984), p. 175.
[2] K. Svozil, Am. J. Phys. **74**, 800 (2006).
[3] J. S. Bell, Physics **1**, 195 (1964).
[4] S. Kochen and E. P. Specker, J. Math. Mech. **17**, 59 (1967).
[5] A. K. Ekert, Phys. Rev. Lett. **67**, 661 (1991).
[6] J. Barrett, L. Hardy, and A. Kent, Phys. Rev. Lett. **95**, 010503 (2005).
[7] A. Acín *et al.*, Phys. Rev. Lett. **98**, 230501 (2007).
[8] W. Rosenfeld *et al.*, Adv. Sci. Lett. **2**, 469 (2009).
[9] A. Cabello, Phys. Rev. Lett. **104**, 220401 (2010).
[10] K. Horodecki *et al.*, e-print arXiv:1006.0468.
[11] K. Svozil, in *Physics and Computation 2010*, edited by H. Guerra (University of Azores, Portugal, Ponta Delgada, 2010), p. 235.
[12] A. Cabello, J. M. Estebaranz, and G. García-Alcaine, Phys. Lett. A **212**, 183 (1996).
[13] E. Nagali, L. Sansoni, L. Marrucci, E. Santamato, and F. Sciarrino, Phys. Rev. A **81**, 052317 (2010).
[14] E. Nagali *et al.*, Phys. Rev. Lett. **105**, 073602 (2010).
[15] M. W. Beijersbergen, L. Allen, H. E. L. O. van der Veen, and J. P. Woerdman, Opt. Commun. **96**, 123 (1993).
[16] E. Nagali *et al.*, Opt. Express **17**, 18745 (2009).
[17] E. Nagali *et al.*, Phys. Rev. Lett. **103**, 013601 (2009).
[18] S. Slussarenko *et al.*, Opt. Express **19**, 4085 (2011).
[19] E. Karimi *et al.*, Opt. Lett. **21**, 3053 (2007).
[20] S. Slussarenko, V. D'Ambrosio, B. Piccirillo, L. Marrucci, and E. Santamato, Opt. Express **18**, 27205 (2010).
[21] H. Wei *et al.*, Opt. Commun. **223**, 117 (2003).

Experimental Observation of Impossible-to-Beat Quantum Advantage on a Hybrid Photonic System

Eleonora Nagali,[1] Vincenzo D'Ambrosio,[1] Fabio Sciarrino,[1,*] and Adán Cabello[2,3,†]
[1]*Dipartimento di Fisica della "Sapienza" Università di Roma, Roma 00185, Italy*[‡]
[2]*Departamento de Física Aplicada II, Universidad de Sevilla, E-41012 Sevilla, Spain*
[3]*Department of Physics, Stockholm University, S-10691 Stockholm, Sweden*
(Received 16 October 2011; published 27 February 2012)

Quantum resources outperform classical ones for certain communication and computational tasks. Remarkably, in some cases, the quantum advantage cannot be improved using hypothetical postquantum resources. A class of tasks with this property can be singled out using graph theory. Here we report the experimental observation of an impossible-to-beat quantum advantage on a four-dimensional quantum system defined by the polarization and orbital angular momentum of a single photon. The results show pristine evidence of the quantum advantage and are compatible with the maximum advantage allowed using postquantum resources.

DOI: 10.1103/PhysRevLett.108.090501 PACS numbers: 03.67.−a, 03.65.Ud, 42.50.Tx, 42.50.Xa

Introduction.—The search for properties singling out quantum mechanics from more general theories has recently attracted much attention [1–8]. In this framework, it is natural to address questions such as which is the simplest task in which quantum mechanics provides an advantage over classical theories and no hypothetical postquantum theory can do it better. The only requirement defining these postquantum theories is that they cannot assign a value larger than 1 to the sum of probabilities of mutually exclusive possibilities. Some recent results have shed light on this problem. Let us consider the class of tasks requiring one to maximize a sum Σ of probabilities of propositions tested on a system (this class includes some communication complexity tasks [9] and all noncontextual [10–12] and Bell inequalities). In Ref. [13] it is shown that the maximum of Σ is given by $C(G)$, $Q(G)$, or $P(G)$, depending on whether classical, quantum, or general resources are used. This numbers are three properties of the graph G in which vertices represent propositions and edges link exclusive propositions. The simplest task of this class in which there is a quantum advantage but no postquantum theory outperforms quantum mechanics corresponds to the simplest graph such that $C(G) < Q(G) = P(G)$, requiring a quantum system with the lowest possible dimensionality $\chi(G)$.

In this Letter we experimentally implement the simplest task with quantum but no postquantum advantage. For this purpose we exploit the properties of the graph of Fig. 1, identified in [14] as the simplest one with these properties, to perform an experiment in which quantum mechanics gives a larger Σ than classical theories and no postquantum theory can do it better. Specifically, for the graph in Fig. 1, $C(G) = 3$ while $Q(G) = P(G) = 3.5$ with $\chi(G) = 4$. Experimentally we adopt a photonic hybrid system of dimension four, encoded in the polarization and a bidimensional subspace of the orbital angular momentum. The high fidelity and reliability of the present scheme allow us to achieve a close to theory measured value and a direct test of the exclusivity of the 10 involved orthogonal projectors.

There is a one-to-one correspondence between $C(G)$, $Q(G)$, and $P(G)$ and the classical, quantum, and general bounds for the following task: given an $n(G)$-vertex graph G, each player is asked to prepare a physical system and provide a list of $n(G)$ yes-no questions (or tests) Q_i on this system, satisfying that questions corresponding to adjacent vertices in G cannot both have the answer yes. The player who provides the preparation and questions with the highest probability of obtaining a yes answer when one question is picked at random wins.

If the questions refer to preexisting properties, that is, all the answers have a predefined value, the highest probability of obtaining a yes answer is $C(G)/n(G)$. For the graph in Fig. 1, the sum of the probabilities of obtaining a yes answer is

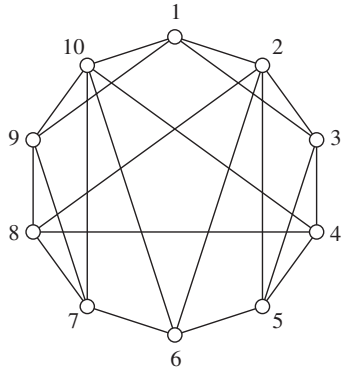

FIG. 1. Graph representing the simplest task of the class defined in the main text with quantum but no postquantum advantage. Vertices represent propositions, edges link propositions that cannot be simultaneously true.

$$\Sigma = \sum_{i=1}^{10} P(Q_i = 1) \leq 3 = C(G), \tag{1}$$

since at most 3 of the questions in Fig. 1 can be true. An optimal classical strategy to win is described in the Supplemental Material [15].

However, in quantum mechanics, preparing a four-level system in the state

$$\langle \psi | = (0, 0, 0, 1), \tag{2}$$

and testing the propositions represented by the projectors $|v_i\rangle\langle v_i|$ over the following 10 (non-normalized) vectors $\langle v_i|$,

$$\langle v_1| = (0, 0, 1, 1), \tag{3a}$$
$$\langle v_2| = (1, -1, 1, -1), \tag{3b}$$
$$\langle v_3| = (1, -1, -1, 1), \tag{3c}$$
$$\langle v_4| = (1, 0, 0, -1), \tag{3d}$$
$$\langle v_5| = (1, 1, 1, 1), \tag{3e}$$
$$\langle v_6| = (0, 1, 0, -1), \tag{3f}$$
$$\langle v_7| = (-1, 1, 1, 1), \tag{3g}$$
$$\langle v_8| = (1, 0, 0, 1), \tag{3h}$$
$$\langle v_9| = (1, 1, 1, -1), \tag{3i}$$
$$\langle v_{10}| = (1, 1, -1, 1), \tag{3j}$$

the probability of obtaining a yes answer is $\frac{7}{20} = 0.35$, which is the maximum using quantum resources [namely, $Q(G)/n(G)$], since for the graph in Fig. 1,

$$Q(G) = \tfrac{7}{2}, \tag{4}$$

which does not only go beyond the classical limit, but actually saturates the bound for any postquantum theory. The simplest way to grasp the previous bound is to notice that any other assignment of probabilities to the vertices of the graph in Fig. 1 either does not beat $7/2$ or is inconsistent with the requirement that the sum of probabilities of mutually adjacent vertices (i.e., those representing mutually exclusive propositions) cannot be larger than 1. As explained in [13], there is a one-to-one correspondence between the maximum of the sum of the probabilities and the so-called fractional packing number of the graph in which vertices represent propositions and edges exclusiveness. The fractional packing number of the graph in Fig. 1 is $7/2$. The remarkable property of the graph in Fig. 1 is that $Q(G) = P(G)$, so no postquantum theory can improve this performance. Unlike standard Bell tests where hypothetical postquantum theories can outperform quantum mechanics [16], here quantum mechanics reaches the maximum performance allowed by the laws of probability, as in this case there is no way to assign probabilities outperforming the quantum ones without violating that the sum of the probabilities of exclusive propositions cannot be higher than 1. Indeed, what makes this experiment special is that it aims to the simplest scenario where the quantum probabilities exhibit this curious property.

Experimental implementation.—To experimentally verify the quantum predictions we require a four-dimensional system and the ability to project ququart states over all the states in Eqs. (3) with high fidelity and high reliability. These states are found to belong to all the five different mutually unbiased bases of a ququart [17,18]. We encoded such higher-dimensional quantum states by exploiting two different degrees of freedom of the same photon. It has been recently demonstrated that ququart states can be efficiently generated by manipulating the polarization and orbital angular momentum (OAM) [19]. The orbital angular momentum of light is related to the photon's transverse-mode spatial structure [20] and can be exploited for implementing qudits encoded in a single photon state [21–23]. The combined use of different degrees of freedom of a photon, such as OAM and spin, enables the implementation of entirely new quantum tasks [24]. Moreover, the implementation of a ququart state by exploiting both the polarization and a bidimensional subspace of orbital angular momentum with fixed OAM eigenvalue $|m|$, the so-called hybrid approach, does not require interferometric stability and is not affected by decoherence due to different Gouy phase for free propagation [25].

Here we considered a bidimensional subset of the infinite-dimensional OAM space, denoted as o_2, spanned by states with OAM eigenvalue $m = \pm 2$ in units of $\hbar$. According to the nomenclature $|\varphi, \phi\rangle = |\varphi\rangle_\pi |\phi\rangle_{o_2}$, where $|\cdot\rangle_\pi$ and $|\cdot\rangle_{o_2}$ stand for the photon quantum state "kets" in the polarization and OAM degrees of freedom, respectively, the logic ququart basis can be written as

$$\{|H, +2\rangle, |H, -2\rangle, |V, +2\rangle, |V, -2\rangle\}, \tag{5}$$

where H (V) refers to horizontal (vertical) polarization. According to these definitions, a generic ququart state expressed as (a_1, a_2, a_3, a_4), as in (3), can be experimentally implemented as

$$a_1|H, +2\rangle + a_2|H, -2\rangle + a_3|V, +2\rangle + a_4|V, -2\rangle. \tag{6}$$

Analogously to [19], the manipulation of the OAM degree of freedom has been achieved by adopting the q-plate device [25,26]. On the polarization, the q plate acts as a half-wave plate, while on the OAM it imposes a shift on the eigenvalue $m = \pm 2q$, where q is an integer or half-integer number determined by the (fixed) pattern of the optical axis of the device. In our experiments we adopted a q plate with $q = 1$, thus manipulating the OAM subspace $o_2 = \{|+2\rangle, |-2\rangle\}$. Interestingly, the ability of the q plate to entangle and disentangle the OAM-polarization degrees of freedom can be exploited for the preparation as well as for the measurement of any ququart states.

Let us briefly give an example of how the q plate works. By injecting a photon in the state $|R\rangle_\pi|0\rangle_o$ ($|L\rangle_\pi|0\rangle_o$), where $|R\rangle_\pi$ ($|L\rangle_\pi$) refers to the right (left) circular polarization, the output state reads $|L\rangle_\pi|-2\rangle_{o_2}$ ($|R\rangle_\pi|+2\rangle_{o_2}$).

TABLE I. Theoretical predictions and experimental results for the probabilities of the different outcomes from measurements on state $(0, 0, 0, 1) = |V, -2\rangle$. We associate to each projection a number used later to identify the state. In the column labeled Type we specify if the state is separable (S) or entangled (E).

State projection	Code	Type	Probabilities Theory	Probabilities Experiment
$(0, 0, 1, 1)$	1	S	1/2	0.69 ± 0.02
$(1, -1, 1, -1)$	2	S	1/4	0.160 ± 0.007
$(1, -1, -1, 1)$	3	S	1/4	0.145 ± 0.006
$(1, 0, 0, -1)$	4	E	1/2	0.44 ± 0.01
$(1, 1, 1, 1)$	5	S	1/4	0.33 ± 0.01
$(0, 1, 0, -1)$	6	S	1/2	0.49 ± 0.01
$(-1, 1, 1, 1)$	7	E	1/4	0.160 ± 0.007
$(1, 0, 0, 1)$	8	E	1/2	0.51 ± 0.01
$(1, 1, 1, -1)$	9	E	1/4	0.34 ± 0.01
$(1, 1, -1, 1)$	10	E	1/4	0.218 ± 0.008
		Sum	7/2	3.49 ± 0.03

It follows from the latter relations that by injecting on a q plate a photon with null OAM value and horizontal polarization, the state $(|R, +2\rangle + |L, -2\rangle)/\sqrt{2}$ is generated, corresponding to a single photon entangled state between two different degrees of freedom. In Table I we report the projections over the ten ququart states on the input state $(0, 0, 0, 1) = |V, -2\rangle$ needed to obtain the maximum possible violation in quantum mechanics.

The experimental setup adopted for such measurements is shown in Fig. 2. A spontaneous parametric source (SPDC) generates heralded single photon states, sent through single mode (SM) fiber to setup (a) in order to encode the input state $(0, 0, 0, 1)$, generated adopting a quantum transferrer $\pi \rightarrow o_2$. This tool allows us to transfer the information initially encoded in the polarization degree of freedom to the OAM, by exploiting the features of the q-plate device combined to a polarizing beam splitter (PBS) [26]. In particular, the input state has been generated by adopting the experimental setup in Fig. 2(a), where the wave plates 1 were oriented to generate right circular polarization, and the settings of wave plates 2 for vertical polarization. Then, measurements have been carried out adopting the setups in Figs. 2(c) and 2(d), depending on whether the state on which the projection had to be carried out was separable or entangled. For the projection on separable states (denoted by S in Table I), we adopted a deterministic transferrer $o_2 \rightarrow \pi$ based on a Sagnac interferometer with a Dove's prism in one of its arms [27]. Thanks to this setup, any qubit encoded in a bidimensional subspace of OAM $|\varphi\rangle_{o_2}$ is transferred to the polarization with probability $p = 1$. When the analysis on entangled states has to be carried out, it is possible to exploit the capability of the q plate to disentangle the polarization to the OAM of a single photon. Indeed, for such projections we adopted a q plate and a standard polarization analysis setup. The experimental results are reported in Table I and compared to the theoretical value of 3.5. We observed a good agreement with the theoretical expectations, thus demonstrating the advantage of adopting quantum resources over classical ones.

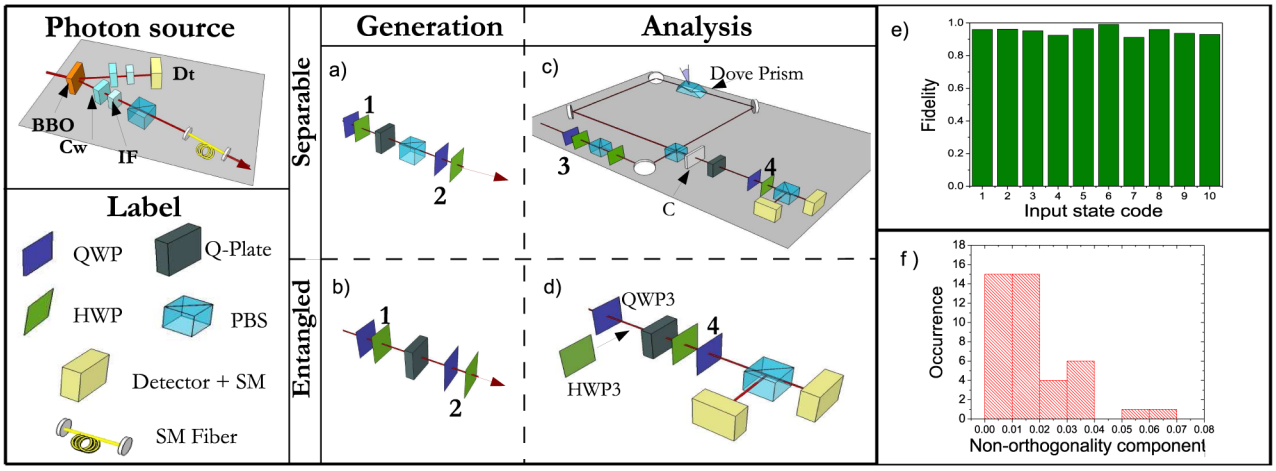

FIG. 2 (color online). Experimental setup for the measurement of the probabilities $p_{i,j}$. In the upper left corner is represented the single photon source, based on spontaneous parametric down-conversion in a nonlinear crystal (BBO) cut for type II SPDC generation of photon pairs and the compensation for the walk-off (C_w) followed by two interference filters (IF) with bandwidth $\Delta\lambda = 3$ nm. See the Supplemental Material [15] for further details. The four schemes we used for the experiment are presented in the central part of the figure. Each state is prepared by one of the two setups of the "Generation" column: Setup (a) for separable states (quantum transferrer $\pi \rightarrow o_2$) and setup (b) for entangled ones [an "entangler" based on a q plate, a quarter-wave plate (QWP), and a half-wave plate (HWP)]. The "Analysis" column shows the setups for the projection on the desired state. Setup (c) for separable states, a deterministic transferrer $o_2 \rightarrow \pi$ (here C is a compensation stage), and setup (d) for entangled states, where a q plate is needed to have a deterministic detection. (e) Experimental fidelities of generation and analysis for the ten states of the graph in Fig. 1. (f) Experimental results of the exclusiveness test: occurrences of the nonorthogonality component of the experimental projectors adopted for the measurements. All measured values of $p(i, j)$ and $p(j, i)$ are reported in the Supplemental Material [15].

As a second step, we provide the experimental verification of exclusiveness relations between the different states in (3), that is, the fact that states connected by an edge cannot be simultaneously both true. We denote by a number from 1 to 10 the states involved in the experiment, and measured the probabilities $p(i, j)$ and $p(j, i)$, where $i, j = 1, \ldots, 10$. For the generation of ququart states belonging to entangled bases, we adopted the scheme reported in Fig. 2(b). In Fig. 2(e) we report the experimental values of probabilities $p(i, i)$, measured in order to ensure a high fidelity in the generation and reliability of all ququart states involved in the experiment. In particular, we observed an average fidelity of $F = (0.9492 \pm 0.0001)$. To verify that experimentally we implement orthogonal projectors, we measured the probabilities $p(i, j)$ and $p(j, i)$ with $i \neq j$. In Fig. 2(f) we report the histogram of the occurrence of different values of probabilities, that quantify the nonorthogonality component of the experimental projectors. We observe a good agreement with the null value expected for orthogonal states. Error bars have been evaluated by considering the Poissonian statistics of photon events.

Discussion.—The classical inequality (1) is valid under the assumption that the measured propositions satisfy the exclusiveness relations given by the graph in Fig. 1. The results in Fig. 2(f) show a very good agreement with the assumption. Even if the agreement between the experimental sum of probabilities is high, for some probabilities the deviations from the theoretical results are larger than the error bars. We attribute such discrepancy to the experimental implementation of the projectors, whose orientation with respect to the input state is slightly different from the expected one. Assuming that inequality (1) is only valid with probability $1 - \epsilon$ and assuming that the worst case scenario, in which there are no links so the bound of the inequality is 10, occurs with probability ϵ, to certify the quantum advantage it is enough that $3(1 - \epsilon) + 10\epsilon < 3.49$; that is, $\epsilon < 0.071$. The impossible-to-beat quantum advantage is certified by the fact that all our 42 experimental probabilities satisfy this condition and by the fact that the average value of ϵ is 0.016 ± 0.001. To our knowledge, this is the first time an experiment performing a task with quantum but no post-quantum advantage [16,28,29] has shown results which demonstrate the quantum advantage and are compatible with the impossibility of a better performance.

In summary, in this Letter we reported the experimental implementation of the simplest impossible-to-beat quantum advantage by adopting a photonic system of dimension four. Such a system has been implemented by exploiting the polarization and orbital angular momentum of single photons. We found a good agreement with theoretical expectation values. Moreover, we have experimentally verified all the exclusiveness relations between the states that correspond to the elements of the graph that models our system.

This work was supported by the MICINN Project No. FIS2008-05596, the Wenner-Gren Foundation, FIRB Futuro in Ricerca-HYTEQ, and Project PHORBITECH of the Future and Emerging Technologies (FET) program within the Seventh Framework Programme for Research of the European Commission, under FET-Open Grant No. 255914.

*fabio.sciarrino@uniroma1.it
†adan@us.es
‡http://quantumoptics.phys.uniroma1.it

[1] L. Hardy, arXiv:quant-ph/0101012.
[2] M. Pawłowski *et al.*, Nature (London) **461**, 1101 (2009).
[3] J. Oppenheim and S. Wehner, Science **330**, 1072 (2010).
[4] B. Dakić and Č. Brukner, in *Deep Beauty: Understanding the Quantum World through Mathematical Innovation*, edited by H. Halvorson (Cambridge University Press, New York, 2011), p. 365.
[5] L. Masanes and M. P. Müller, New J. Phys. **13**, 063001 (2011).
[6] G. Chiribella, G. M. D'Ariano, and P. Perinotti, Phys. Rev. A **84**, 012311 (2011).
[7] H. Barnum, S. Beigi, S. Boixo, M. B. Elliott, and S. Wehner, Phys. Rev. Lett. **104**, 140401 (2010).
[8] G. de la Torre, L. Masanes, A. J. Short, and M. Müller, arXiv:1110.5482.
[9] Č. Brukner, M. Żukowski, J.-W. Pan, and A. Zeilinger, Phys. Rev. Lett. **92**, 127901 (2004).
[10] A. Cabello, Phys. Rev. Lett. **101**, 210401 (2008).
[11] G. Kirchmair *et al.*, Nature (London) **460**, 494 (2009).
[12] E. Amselem, M. Rådmark, M. Bourennane, and A. Cabello, Phys. Rev. Lett. **103**, 160405 (2009).
[13] A. Cabello, S. Severini, and A. Winter, arXiv:1010.2163.
[14] A. Cabello, L. E. Danielsen, A. J. López-Tarrida, and J. R. Portillo, http://www.ii.uib.no/~larsed/quantum_graphs/.
[15] See Supplemental Material at http://link.aps.org/supplemental/10.1103/PhysRevLett.108.090501 for an optimal classical strategy to win, further details on the experimental setup, and experimental results of the exclusiveness test.
[16] L. Aolita *et al.*, arXiv:1105.3598.
[17] A. Klappenecker and M. Rötteler, in *International Conference on Finite Fields and Applications*, edited by G. L. Mullen, A. Poli, and H. Stichtenoth, Lecture Notes in Computer Science Vol. 2984 (Springer, Berlin, 2004), p. 137.
[18] M. Planat and A. C. Baboin, J. Phys. A **40**, F1005 (2007).
[19] E. Nagali, L. Sansoni, L. Marrucci, E. Santamato, and F. Sciarrino, Phys. Rev. A **81**, 052317 (2010).
[20] L. Allen, M. W. Beijersbergen, R. J. C. Spreeuw, and J. P. Woerdman, Phys. Rev. A **45**, 8185 (1992).
[21] S. Franke-Arnold, L. Allen, and M. Padgett, Laser Photon. Rev. **2**, 299 (2008).
[22] G. Molina-Terriza, J. P. Torres, and L. Torner, Nature Phys. **3**, 305 (2007).
[23] S. S. R. Oemrawsingh *et al.*, Phys. Rev. Lett. **95**, 240501 (2005).
[24] J. T. Barreiro *et al.*, Nature Phys. **4**, 282 (2008).
[25] E. Nagali *et al.*, Opt. Express **17**, 18745 (2009).
[26] E. Nagali *et al.*, Phys. Rev. Lett. **103**, 013601 (2009).
[27] V. D'Ambrosio *et al.*, Opt. Lett. **37**, 172 (2012).
[28] J. Zhang *et al.*, Phys. Rev. A **75**, 022302 (2007).
[29] P. Kolenderski *et al.*, arXiv:1107.5828.

Experimental implementation of a Kochen-Specker set of quantum tests

Vincenzo D'Ambrosio,[1] Isabelle Herbauts,[2] Elias Amselem,[2] Eleonora Nagali,[1]
Mohamed Bourennane,[2] Fabio Sciarrino,[1] and Adán Cabello[3,2]

[1]*Dipartimento di Fisica della "Sapienza" Università di Roma, Roma 00185, Italy*
[2]*Department of Physics, Stockholm University, S-10691 Stockholm, Sweden*
[3]*Departamento de Física Aplicada II, Universidad de Sevilla, E-41012 Sevilla, Spain*

(Dated: September 11, 2012)

The conflict between classical and quantum physics can be identified through a series of yes-no tests on quantum systems, without it being necessary that these systems be in special quantum states. Kochen-Specker (KS) sets of yes-no tests have this property and provide a quantum vs classical advantage, free of the initialization problem affecting quantum computers. Here we report the first experimental implementation of a complete KS set consisting of 18 yes-no tests on four-dimensional quantum systems, and show how to use them to obtain state-independent quantum advantage. We first demonstrate the unique power of this KS set for solving a task avoiding the problem of state initialization. This is done by showing that, for 28 different quantum states encoded in the orbital angular momentum and polarization degrees of freedom of single photons, the KS set provide an impossible-to-beat solution. In a second experiment, we generate maximally contextual quantum correlations by performing compatible sequential measurements of the polarization and path of single photons. In this case, state-independence is demonstrated for 15 different initial states. Maximum contextuality and state-independence follow from the fact that the sequences of measurements project any initial quantum state onto one of the KS set's eigenstates. Our results show that KS sets can be used for quantum information processing and quantum computation, and pave the way for future developments.

I. INTRODUCTION

The classical description of nature is based on the assumption that all physical systems possess properties, such as position and velocity, that can be revealed by the act of observation and whose objective existence is independent of whether or not the observation does actually take place. A consequence of this assumption is that there should exist a joint probability distribution for the results of any set of joint measurements revealing these properties [1]. However, there is a fundamental theorem that states that, if quantum mechanics (QM) is correct, then nature cannot be described in classical terms [2–4]. Kochen and Specker (KS) provided a particularly appealing proof of this theorem [4], valid for systems in any quantum state and which therefore does not require the system to be prepared in specific quantum states, as is the case for the violation of Bell inequalities [5].

KS proved that, for any quantum system of dimension $d \geq 3$, there are sets of yes-no tests (represented in QM by projectors $\Pi_i = |v_i\rangle\langle v_i|$ onto unit vectors $|v_i\rangle$) for which it is impossible to assign results 1 (yes) or 0 (no) in agreement with two predictions of QM: (i) If two exclusive tests (represented by orthogonal projectors) are performed on the same system, both cannot give the result 1. (ii) If d pairwise exclusive tests (i.e., satisfying $\sum_{i=1}^{d} \Pi_i = \mathbb{I}$, with $\mathbb{I}$ the d-dimensional identity matrix) are performed on the same system, then one of the tests gives 1. For a given d, these sets, called KS sets, are universal in the sense that assigning results is impossible for *any* quantum state. The existence of KS sets demonstrates that, for any quantum state, it is impossible to reproduce the predictions of QM with theories in which the measurement results are independent of other compatible measurements. These theories are called non-contextual hidden variable (NCHV) theories.

The original KS set had 117 yes-no tests in $d = 3$ [4]. In $d = 3$, the simplest known KS set has 31 tests [6] and it has been proven that a KS set with less than 19 tests does not exist [7–9]. Indeed, numerical evidence suggests there is no KS set with less than 22 tests in $d = 3$ [7]. However, in $d = 4$, there is a KS set with 18 yes-no tests [10], and it has been proven that there is no KS set with a smaller number of yes-no tests [7, 9]. Moreover, there is numerical evidence that the same holds for any dimension [7], suggesting that, as conjectured by Peres [11], the 18-test KS set is the simplest one in any dimension. A graph can be associated to any KS set [4]. In this graph, each yes-no test of the KS set is represented by a vertex and exclusive yes-no tests are represented by adjacent vertices. Fig. 1 a) shows the graph corresponding to the 18-test KS set. Other proofs of state-independent quantum contextuality based on observables represented by Pauli operators [12, 13] can be expressed in terms of KS sets, by noticing that the projectors onto the common eigenstates of the commuting Pauli operators constitute a KS set [14, 15].

While Bell inequalities [5] have stimulated a large number of experiments (e.g., [16–19]) and have a number of applications (e.g., [20–22]), KS sets of yes-no questions have never been implemented experimentally.

II. EXPERIMENTAL OBSERVATION OF STATE-INDEPENDENT IMPOSSIBLE-TO-BEAT KS-BASED QUANTUM ADVANTAGE USING POLARIZATION AND ORBITAL ANGULAR MOMENTUM OF PHOTONS

Consider the following task [23]: Given an n-vertex graph G, provide n yes-no tests about a physical system, such that each test is associated to a vertex of G, exclusive tests correspond to adjacent vertices, and such that these tests result in the highest probability of obtaining a yes answer when one of them is chosen at random. This highest probability may be different depending on whether the physical system and the tests are classical, quantum, or post-quantum. Moreover, for arbitrary graphs, the highest probability may also depend on the state in which the system is prepared. However, two distinguishing features of the graph of Fig. 1 a) are that the highest probability in QM can be reached regardless of the state of the system, and cannot be outperformed by any post-quantum theory (see Supplementary information).

If the available resources are classical, i.e., physical systems with preassigned results and tests thereof, then an optimal strategy is illustrated in Fig. 1 b). There, the classical system is assumed to be a ball that can be placed in one out of 18 boxes numbered from 1 to 18. For instance, a yes-no test is: "Is the ball in box 1 or in box 2 or in box 11 or in box 16?", denoted as "1, 2, 11, 16". The other tests are shown in Fig. 1 b). The 18 tests satisfy the graph's relations of exclusive disjunction. In addition, no matter which box the ball is placed in, the probability of getting a yes answer when one of the 18 tests is chosen at random is $4/18 \approx 0.22$, since the answer is always "yes" for 4 of the tests and "no" for the others. Alternatively, the performance can be measured by the sum Σ of the probabilities of obtaining a yes answer. It can be proven that, for this graph, no other set of classical yes-no tests allows a higher probability (see Supplementary information). Therefore, using classical resources,

$$\Sigma = \sum_{i \in V(G)} P(\Pi_i = 1) \leq 4. \tag{1}$$

where $V(G)$ is the set of vertices of the graph in Fig. 1 a) and $P(\Pi_i = 1)$ is the probability of obtaining the result 1 (yes) for the yes-no test Π_i.

However, it can be easily checked that, if we use the 18 quantum yes-no tests $\Pi_i = |v_i\rangle\langle v_i|$ in Fig. 1 a), then the probability of a yes answer is $1/4 = 0.25$ and

$$\Sigma_{\mathrm{QM}} = 4.5. \tag{2}$$

Since this advantage is independent of the initial quantum state of the system, this is an example of a task with quantum advantage for which the initialization problem affecting some quantum computers [24, 25] is not an obstacle. Moreover, for this task, even hypothetical post-quantum theories cannot outperform QM (see Supplementary information).

In order to test this state-independent impossible-to-beat quantum advantage in an experiment, we used for the encoding two different degrees of freedom of the same photon: the polarization and a bidimensional subset of the orbital angular momentum (OAM) space [26], spanned by the states with eigenvalues $m = \pm 2\hbar$. The four-dimensional logical basis for encoding is

$$\{|H, +2\rangle, |H, -2\rangle, |V, +2\rangle, |V, -2\rangle\}, \tag{3}$$

where H and V denote horizontal and vertical polarization, respectively, and ± 2 denotes $m = \pm 2\hbar$.

The experimental setup involves preparing the required states (preparation stage) and then projecting them onto the desired states (measurement stage). In the preparation stage, the light from a heralded single photon source at 795 nm, based on non-collinear spontaneous parametric down conversion (SPDC) in a beta barium borate crystal pumped by the second harmonic of a femtosecond pulsed laser with repetition rate 76 MHz, is coupled to a single mode (SM) fiber in order to project the OAM of the generated photons in the transverse electromagnetic TEM_{00} mode (which is an OAM eigenstate with eigenvalue equal to zero). The second photon generated in the SPDC acts as a trigger of the single photon generation. After the SM fiber, the input photon is prepared using half waveplates (HWPs), quarter waveplates (QWPs), q-plates (QPs), and polarizing beam splitters (PBSs) to generate the required states in the logical basis (3). As explained in Fig. 2, the procedure is different depending on whether the state to be generated is separable or entangled.

The QPs are liquid crystal devices that produce a spin-orbit coupling of the polarization and OAM contributions to the photons' total angular momentum [27]. When a photon interacts with the QP, it suffers an exchange of OAM driven by the input polarization. In particular, for the QPs adopted in this experiment, the shift of OAM is equal to $\pm 2\hbar$ when the input photon has left (right) polarization [28, 29]. The QP efficiency has been optimized by controlling the electrical tuning [30], leading to a conversion efficiency of 94%. Thanks to its features, the QP can be adopted both for generating and analysing of quantum states encoded in the OAM.

The measurement stage is achieved by using a deterministic transferrer based on a Sagnac interferometer, with a Dove prism in one of the arms when the prepared state is separable [31], and with a QP with a standard polarization analysis setup when the state is entangled. For each state to be analyzed, we recorded the coincidence counts between the trigger and the signal coupled through the SM fiber at the end of the measurement setup. Considering all losses contributions in the setup, we recorded around 30 Hz as mean coincidence counts. The experimental results for Σ, as measured on 15 different states, are reported in Table I. The experimental data are in good agreement with the theoretical predic-

tion, with a mean value of $\Sigma_{exp} = 4.512 \pm 0.005$ to be compared to $\Sigma = 4.5$, and shows the clear advantage of the quantum settings with KS projectors over any classical strategy.

Code	State	Implementation	Σ
v_1	(1,0,0,0)	$\|H,+2\rangle$	4.60 ± 0.02
v_2	(0,1,0,0)	$\|H,-2\rangle$	4.45 ± 0.02
v_7	(1,1,1,1)	$\|A,h\rangle$	4.50 ± 0.02
v_{11}	(1,0,1,0)	$\|A,+2\rangle$	4.51 ± 0.02
v_{15}	(1,0,0,1)	$\|\psi_1\rangle = \frac{1}{\sqrt{2}}(\|H,+2\rangle + \|V,-2\rangle)$	4.59 ± 0.02
v_{16}	(0,1,-1,0)	$\|\psi_3\rangle = \frac{1}{\sqrt{2}}(\|H,-2\rangle - \|V,+2\rangle)$	4.47 ± 0.01
v_{17}	(0,1,1,0)	$\|\psi_4\rangle = \frac{1}{\sqrt{2}}(\|H,-2\rangle + \|V,+2\rangle)$	4.41 ± 0.02
v_{18}	(0,0,0,1)	$\|V,-2\rangle$	4.50 ± 0.02
v_{19}	(0,0,1,0)	$\|V,+2\rangle$	4.45 ± 0.03
v_{20}	(1,1,0,0)	$\|H,h\rangle$	4.57 ± 0.02
v_{24}	(1,0,0,-1)	$\|\psi_2\rangle = \frac{1}{\sqrt{2}}(\|H,+2\rangle - \|V,-2\rangle)$	4.58 ± 0.02
ρ_{25}		$\frac{13}{16}\|\psi_1\rangle\langle\psi_1\| + \frac{1}{16}\sum_{j=2}^{4}\|\psi_j\rangle\langle\psi_j\|$	4.57 ± 0.02
ρ_{26}		$\frac{5}{8}\|\psi_1\rangle\langle\psi_1\| + \frac{1}{8}\sum_{j=2}^{4}\|\psi_j\rangle\langle\psi_j\|$	4.55 ± 0.02
ρ_{27}		$\frac{7}{16}\|\psi_1\rangle\langle\psi_1\| + \frac{3}{16}\sum_{j=2}^{4}\|\psi_j\rangle\langle\psi_j\|$	4.53 ± 0.02
ρ_{28}		$\frac{1}{4}\sum_{j=1}^{4}\|\psi_j\rangle\langle\psi_j\|$	4.50 ± 0.02
Average value			4.512 ± 0.005

TABLE I: **Experimental results for Σ for 15 quantum states.** Each input state was projected onto each of the 18 states in Fig. 1 a). Notation: $|A\rangle = \frac{|H\rangle+|V\rangle}{\sqrt{2}}$, $|h\rangle = \frac{|+2\rangle+|-2\rangle}{\sqrt{2}}$. Error bars were evaluated by considering the Poissonian statistics of coincidence counts. All reported values lie in the range $[\Sigma_{min}, \Sigma_{max}]$ (see Fig. 3).

In addition, the exclusive disjunction between the tests in Fig. 1 a) was experimentally verified, confirming that tests corresponding to adjacent vertices cannot be both simultaneously true. Experimentally, the probabilities $P_{|v_j\rangle}(\Pi_i = 1)$, obtained by projecting the state $|v_i\rangle$ onto the state $|v_j\rangle$ for orthogonal states (adjacent vertices), are close to 0, as expected. Specifically, we obtained that the mean value of $P_{|v_j\rangle}(\Pi_i = 1)$ is $\epsilon = (0.014 \pm 0.001)$ (see Supplementary information).

The theoretical classical and quantum bounds for the task should be properly corrected to take into account that $\epsilon \neq 0$. Assuming that inequality (1) is only valid with probability $1 - \epsilon$ and that the worst case scenario, in which there are no edges so the upper bound of the inequality is 18, occurs with probability ϵ, to certify the quantum advantage it is enough that $4(1-\epsilon) + 18\epsilon < \Sigma$, which, using $\Sigma = 4.5$, implies $\epsilon < 0.035$, a condition which is fulfilled in our experiment. Moreover, we expect to observe a quantum advantage lying in a range $[\Sigma_{min}, \Sigma_{max}]$, where $\Sigma_{min} = 4.5(1-\epsilon)$ and $\Sigma_{max} = 4.5(1-\epsilon) + 18\epsilon$. Here Σ_{max} (Σ_{min}) corresponds to the situation of having all 18 propositions true (false) with probability ϵ. In Fig. 3 we report the experimental values of Σ, not only for the 15 states in Table I, but also for other 13 states. The quantum advantage is observed for all 28 states, in good agreement with the state-independent value predicted by the theory. We note that all experimental values of Σ lie in the expected range $[\Sigma_{min}, \Sigma_{max}]$.

III. EXPERIMENTAL STATE-INDEPENDENT MAXIMALLY CONTEXTUAL QUANTUM CORRELATIONS BY SEQUENTIAL MEASUREMENTS ON POLARIZATION AND PATH OF PHOTONS

KS sets can also be used to generate non-classical contextual correlations by performing sequential compatible measurements on individual systems. The signature of non-classicality is the violation of a non-contextuality inequality, which is an inequality involving linear combinations of joint probabilities of sequential compatible measurements, satisfied by any NCHV theory.

For most of the experimental demonstrations of contextual correlations to date [32–35], the system has to be prepared in a special state. There are also theoretical [36] and experimental works [37–39] on state-independent contextuality. However, none of the previous experiments implement a KS set of yes-no tests.

Here we use the KS set of Fig. 1 a) to obtain a non-contextuality inequality violated by any quantum state. This inequality follows from identifying sequential compatible measurements such that any initial state is projected onto one of the eigenstates of the yes-no tests of the KS set of Fig. 1 a). This guarantees that the propositions $abc|xyz$ denoting "the result of measuring x (first measurement of the sequence) is a, the result of measuring y (second) is b, and the result of measuring z (third) is c" keep all the relations of exclusive disjunction existing in Fig. 1 a).

It can be easily seen that, by using the following measurements:

$$\begin{aligned} &0 := \sigma_z \otimes \mathbb{I}, \quad &&1 := \mathbb{I} \otimes \sigma_z, \quad &&2 := \sigma_z \otimes \sigma_z, \\ &3 := \mathbb{I} \otimes \sigma_x, \quad &&4 := \sigma_x \otimes \mathbb{I}, \quad &&5 := \sigma_x \otimes \sigma_x, \\ &6 := \sigma_z \otimes \sigma_x, \quad &&7 := \sigma_x \otimes \sigma_z, \quad &&8 := \sigma_y \otimes \sigma_y, \end{aligned} \tag{4}$$

where σ_x, σ_y, and σ_z are the Pauli matrices along the x, y, and z directions, $\otimes$ denotes tensor product, and assigning the results 0 and 1 to the degenerate eigenvalues -1 and 1 of the operators, the 18 propositions in Fig. 1 c) are in one-to-one correspondence with the 18 states in Fig. 1 a). Therefore, the corresponding non-contextuality

inequality reads

$$\begin{aligned}\xi =& P(001|012) + P(111|012) + P(100|012) \\ &+ P(010|036) + P(001|036) + P(100|036) \\ &+ P(100|345) + P(111|345) + P(010|345) \\ &+ P(100|147) + P(001|147) + P(111|147) \\ &+ P(100|678) + P(001|678) + P(111|678) \\ &+ P(110|258) + P(000|258) + P(011|258) \overset{\text{NCHV}}{\leq} 4,\end{aligned} \tag{5}$$

where the upper bound for NCHV theories follows from the classical bound of inequality (1). For any initial state, these sequences of quantum measurements lead to

$$\xi_{\text{QM}} = 4.5, \tag{6}$$

in correspondence with the quantum advantage (2). It can be proven that the contextuality revealed by this violation cannot be outperformed by any post-quantum theory (see Supplementary information).

We tested inequality (5) in a separate experiment using a single four-dimensional system with two qubits encoded in the spatial path and two qubits encoded in the polarization of the photon. For this experiment, the logical basis is

$$\{|t,H\rangle, |t,V\rangle, |r,H\rangle, |r,V\rangle\}, \tag{7}$$

where t and r denote the transmitted and reflected paths of the photon, respectively, and H and V denote horizontal and vertical polarization, respectively.

The experiment involves testing a sequence of three compatible measurements, corresponding to rows or columns in (4). To do so, the experimental setup is designed as a cascade of measurement boxes representing the compatible observables, preceded by a preparation device, and followed by detectors [35, 38]. The preparation device consists of a source of H-polarized single photons, implemented using a narrow bandwidth cw diode laser at 780 nm of long coherence length, attenuated to a mean photon number of 0.06 photons per coincidence gate. Combinations of HWPs, PBSs, and a wedge placed after the single-photon source create any desired state in the logical basis 7. The detection stage uses calibrated silicon avalanche photodiodes, with a 8-channel coincidence logic, and a coincidence window of 1.7 ns.

Crucial for the experimental test of the non-contextuality inequality (5) is the proper design of the devices for measuring the observables in (4). These devices should satisfy two conditions: compatibility [the three measurements corresponding to rows and columns in (4) should be compatible, so that any subsequent measurement of any of them would give the same result] and non-contextuality [every observable in (4) has to be measured using the same device in any of the sequences]. These conditions were achieved with the design of the 9 measuring devices shown in Fig. 4.

To construct the cascade setup, we used displaced Sagnac interferometers with very high stability. We obtained visibilities in the 90%–99% range, depending on the implemented sequence. The detection efficiency of the single-photon detectors was 55% and the efficiency of the fiber coupling was 90%. The experimental value of ξ for 15 different quantum states is reported in Table II. Under the assumption that the detected photons were an unbiased subset of the emitted photons (fair sampling assumption), the results in Table II are in good agreement with a state-independent violation of inequality (5). The deviations from the quantum prediction for an ideal experiment with perfect compatibility are due to the systematic errors arising from the interferometers, the light-mode overlapping, and the imperfection of the polarization components.

Code	**State**	**Implementation**	ξ
v_1	(1,0,0,0)	$\|t,H\rangle$	4.1953 ± 0.0015
v_2	(0,1,0,0)	$\|t,V\rangle$	4.2690 ± 0.0025
v_7	(1,1,1,1)	$\|p,D\rangle$	4.3790 ± 0.0011
v_{11}	(1,0,1,0)	$\|p,H\rangle$	4.4406 ± 0.0024
v_{15}	(1,0,0,1)	$\|\psi_1\rangle = \frac{1}{\sqrt{2}}(\|t,H\rangle + \|r,V\rangle)$	4.2607 ± 0.0011
v_{16}	(0,1,-1,0)	$\|\psi_3\rangle = \frac{1}{\sqrt{2}}(\|r,H\rangle - \|t,V\rangle)$	4.2550 ± 0.0020
v_{17}	(0,1,1,0)	$\|\psi_4\rangle = \frac{1}{\sqrt{2}}(\|r,H\rangle + \|t,V\rangle)$	4.1990 ± 0.0022
v_{18}	(0,0,0,1)	$\|r,V\rangle$	4.3001 ± 0.0017
v_{19}	(0,0,1,0)	$\|r,H\rangle$	4.3346 ± 0.0030
v_{20}	(1,1,0,0)	$\|t,D\rangle$	4.4113 ± 0.0013
v_{24}	(1,0,0,-1)	$\|\psi_2\rangle = \frac{1}{\sqrt{2}}(\|t,H\rangle - \|r,V\rangle)$	4.2468 ± 0.0011
ρ_{25}		$\frac{13}{16}\|\psi_1\rangle\langle\psi_1\| + \frac{1}{16}\sum_{j=2}^{4}\|\psi_j\rangle\langle\psi_j\|$	4.3136 ± 0.0819
ρ_{26}		$\frac{5}{8}\|\psi_1\rangle\langle\psi_1\| + \frac{1}{8}\sum_{j=2}^{4}\|\psi_j\rangle\langle\psi_j\|$	4.3479 ± 0.0984
ρ_{27}		$\frac{7}{16}\|\psi_1\rangle\langle\psi_1\| + \frac{3}{16}\sum_{j=2}^{4}\|\psi_j\rangle\langle\psi_j\|$	4.3171 ± 0.1080
ρ_{28}		$\frac{1}{4}\sum_{j=1}^{4}\|\psi_j\rangle\langle\psi_j\|$	4.3968 ± 0.1098

TABLE II: **Experimental results for ξ for 15 quantum states.** Notation: $|p\rangle = \frac{|t\rangle+|r\rangle}{\sqrt{2}}$, $|D\rangle = \frac{|H\rangle+|V\rangle}{\sqrt{2}}$. The errors in the results of ξ were deduced from the standard deviation of 50 samples in the 10-second time period (see Supplementary information for all the experimental values of $P(abc|xyz)$ for the 15 states).

IV. CONCLUSIONS

We have presented the first experimental implementation of a KS set of quantum yes-no tests in two experiments using two different four-dimensional photonic systems and with two different purposes.

In the first experiment, we used the polarization and orbital angular momentum of single photons to show the quantum vs classical advantage of using a KS set of 18 yes-no tests for a specific task, and demonstrated that this advantage is independent of the state initial-

ization and cannot be outperformed using hypothetical post-quantum resources.

In the second experiment, we performed sequential measurements of compatible observables encoded in the path and polarization degrees of freedom of single photons to show the state-independent violation of a non-contextuality inequality constructed in one-to-one correspondence with the eigenstates of the KS set, showing how KS sets can be used to reveal state-independent maximally contextual quantum correlations.

Our results pave the way for further quantum state-independent applications for quantum information processing and quantum computation. Near-future developments may include cryptographic applications [40, 41], dimension witnessing [42], state-independent quantum correlations with computational power [43], higher dimensionality KS sets [15], and portable KS sets implemented on integrated photonic circuits [44–47].

Acknowledgments

We acknowledge fruitful discussions with A. J. López-Tarrida and thank M. Rådmark for technical support with the experiment. This work was supported by the Spanish Project No. FIS2011-29400, the Wenner-Gren Foundation, FIRB Futuro in Ricerca-HYTEQ, the Swedish Research Council (VR), and Project PHORBITECH of the Future and Emerging Technologies (FET) program within the Seventh Framework Programme for Research of the European Commission, under FET-Open Grant No. 255914.

V. SUPPLEMENTARY INFORMATION

A. Proof that the set of classical tests in Fig. 1 b) provides the maximum probability of obtaining yes using classical resources

The maximum probability of obtaining a result 1 (yes) when a yes-no test is chosen at random and using classical resources is given by $\alpha(G)/n(G)$, where G is the graph defined in the main text, $\alpha(G)$ is its independence number (defined as the maximum number of pairwise nonadjacent vertices in G), and $n(G)$ is the number of vertices of G [48]. For the graph in Fig. 1 b), $\alpha(G) = 4$ and $n(G) = 18$. For the set of classical tests in Fig. 1 b), the probability is 4/18, no matter in which box the ball was initially placed. On the other hand, the minimum number of classical states needed to accomplish the task is given by the intersection number of the complement of G, $\theta'(\bar{G})$ (defined as the smallest number of subsets of pairwise adjacent vertices needed to cover all of the edges of the complement of G). For the graph in Fig. 1 b), $\theta'(\bar{G}) = 18$, which shows that the strategy in Fig. 1 b) is also optimal in the sense that it uses the smallest possible classical system. ■

B. Proof that the highest probability for the task with quantum resources cannot be outperformed using post-quantum resources

The maximum probability of obtaining a result 1 (yes) when a yes-no test is chosen at random and using post-quantum resources is given by $\alpha(G)^*/n(G)$, where $\alpha^*(G)$ is the fractional packing number of G, which is defined as

$$\alpha^*(G) = \max \sum_{i \in V(G)} w_i, \tag{8}$$

where $V(G)$ is the set of vertices of G, and the maximum is taken for all $0 \leq w_i \leq 1$ and for all subsets of pairwise adjacent vertices c_j of G, under the restriction $\sum_{i \in c_j} w_i \leq 1$ [48]. For the graph in Fig. 1 b), $\alpha^*(G) = 4.5$. ■

C. Proof that the highest quantum violation of the non-contextuality inequality (5) cannot be outperformed using post-quantum resources

The highest quantum violation of a non-contextuality inequality which can be expressed as a sum of joint probabilities $P(abc|xyz)$ is given by the Lovász number $\vartheta^(G)$ of the graph in which each proposition $abc|xyz$ is represented by a vertex and exclusive propositions correspond to adjacent vertices [48]. The Lovász number of a graph G is

$$\vartheta(G) = \max \sum_{i \in V(G)} |\langle \psi | v_i \rangle|^2, \tag{9}$$

where the maximum is taken over all unit vectors $|\psi\rangle$ and $|v_i\rangle$ and all dimensions, where each $|v_i\rangle$ corresponds to a vertex of G, and two vertices are adjacent if and only if the corresponding vectors are orthogonal.

On the other hand, the highest violation of a non-contextuality inequality in agreement with the laws of probability is given by $\alpha^*(G)$ [48].

The graph G for the non-contextuality inequality (5) is the one in Fig. 1 c), which has $\vartheta(G) = \alpha^*(G) = 4.5$. ■

[1] Fine, A. I. Joint distributions, quantum correlations, and commuting observables. *J. Math. Phys.* **23**, 1306–1310 (1982).

[2] Specker, E. P. Die Logik nicht gleichzeitig entscheidbarer Aussagen. *Dialectica* **14**, 239–246 (1960).

[3] Bell, J. S. On the problem of hidden variables in quantum

Code	State	Implementation 1	Implementation 2
v_1	$(1,0,0,0)$	$\|H,+2\rangle$	$\|t,H\rangle$
v_2	$(0,1,0,0)$	$\|H,-2\rangle$	$\|t,V\rangle$
v_3	$(0,0,1,1)$	$\|V,h\rangle$	$\|r,A\rangle$
v_4	$(0,0,1,-1)$	$\|V,v\rangle$	$\|r,D\rangle$
v_5	$(1,-1,0,0)$	$\|H,v\rangle$	$\|t,D\rangle$
v_6	$(1,1,-1,-1)$	$\|D,h\rangle$	$\|s,A\rangle$
v_7	$(1,1,1,1)$	$\|A,h\rangle$	$\|p,A\rangle$
v_8	$(1,-1,1,-1)$	$\|A,v\rangle$	$\|p,D\rangle$
v_9	$(1,0,-1,0)$	$\|D,+2\rangle$	$\|s,H\rangle$
v_{10}	$(0,1,0,-1)$	$\|D,-2\rangle$	$\|s,V\rangle$
v_{11}	$(1,0,1,0)$	$\|A,+2\rangle$	$\|p,H\rangle$
v_{12}	$(1,1,-1,1)$	$\frac{1}{\sqrt{2}}(\|D,+2\rangle + \|A,-2\rangle)$	$\frac{1}{\sqrt{2}}(\|t,A\rangle - \|r,D\rangle)$
v_{13}	$(-1,1,1,1)$	$\frac{1}{\sqrt{2}}(\|A,-2\rangle - \|D,+2\rangle)$	$\frac{1}{\sqrt{2}}(\|t,D\rangle - \|r,A\rangle)$
v_{14}	$(1,1,1,-1)$	$\frac{1}{\sqrt{2}}(\|A,+2\rangle + \|D,-2\rangle)$	$\frac{1}{\sqrt{2}}(\|t,A\rangle + \|r,D\rangle)$
v_{15}	$(1,0,0,1)$	$\frac{1}{\sqrt{2}}(\|H,+2\rangle + \|V,-2\rangle)$	$\frac{1}{\sqrt{2}}(\|t,H\rangle + \|r,V\rangle)$
v_{16}	$(0,1,-1,0)$	$\frac{1}{\sqrt{2}}(\|H,-2\rangle - \|V,+2\rangle)$	$\frac{1}{\sqrt{2}}(\|r,H\rangle - \|t,V\rangle)$
v_{17}	$(0,1,1,0)$	$\frac{1}{\sqrt{2}}(\|H,-2\rangle + \|V,+2\rangle)$	$\frac{1}{\sqrt{2}}(\|r,H\rangle + \|t,V\rangle)$
v_{18}	$(0,0,0,1)$	$\|V,-2\rangle$	$\|r,V\rangle$

TABLE III: **Implementations of 18 eigenstates of the KS set used in the experiments 1 and 2.** Notation: $|A\rangle = \frac{|H\rangle+|V\rangle}{\sqrt{2}}$, $|D\rangle = \frac{|H\rangle-|V\rangle}{\sqrt{2}}$, $|h\rangle = \frac{|+2\rangle+|-2\rangle}{\sqrt{2}}$, $|v\rangle = \frac{|+2\rangle-|-2\rangle}{\sqrt{2}}$, $|p\rangle = \frac{|t\rangle+|r\rangle}{\sqrt{2}}$, $|s\rangle = \frac{|t\rangle-|r\rangle}{\sqrt{2}}$. Each state v_i corresponds to a vertex in the graph in Fig. 1 a).

State	Implementation 1	Σ
v_1	$\|H,+2\rangle$	4.60
v_2	$\|H,-2\rangle$	4.45
v_3	$\|V,h\rangle$	4.51
v_4	$\|V,v\rangle$	4.63
v_5	$\|H,v\rangle$	4.54
v_6	$\|D,h\rangle$	4.55
v_7	$\|A,h\rangle$	4.50
v_8	$\|A,v\rangle$	4.45
v_9	$\|D,+2\rangle$	4.48
v_{10}	$\|D,-2\rangle$	4.65
v_{11}	$\|A,+2\rangle$	4.51
v_{12}	$\frac{1}{\sqrt{2}}(\|D,+2\rangle + \|A,-2\rangle)$	4.42
v_{13}	$\frac{1}{\sqrt{2}}(\|A,-2\rangle - \|D,+2\rangle)$	4.51
v_{14}	$\frac{1}{\sqrt{2}}(\|A,+2\rangle + \|D,-2\rangle)$	4.52
v_{15}	$\|\psi_1\rangle = \frac{1}{\sqrt{2}}(\|H,+2\rangle + \|V,-2\rangle)$	4.59
v_{16}	$\|\psi_3\rangle = \frac{1}{\sqrt{2}}(\|H,-2\rangle - \|V,+2\rangle)$	4.47
v_{17}	$\|\psi_4\rangle = \frac{1}{\sqrt{2}}(\|H,-2\rangle + \|V,+2\rangle)$	4.41
v_{18}	$\|V,-2\rangle$	4.50
v_{19}	$\|V,+2\rangle$	4.45
v_{20}	$\|H,h\rangle$	4.57
v_{21}	$\|A,-2\rangle$	4.37
v_{22}	$\|D,v\rangle$	4.45
v_{23}	$\frac{1}{\sqrt{2}}(\|A,+2\rangle - \|D,-2\rangle)$	4.42
v_{24}	$\|\psi_2\rangle = \frac{1}{\sqrt{2}}(\|H,+2\rangle - \|V,-2\rangle)$	4.58
ρ_{25}	$\frac{13}{16}\|\psi_1\rangle\langle\psi_1\| + \frac{1}{16}\sum_{j=2}^{4}\|\psi_j\rangle\langle\psi_j\|$	4.57
ρ_{26}	$\frac{5}{8}\|\psi_1\rangle\langle\psi_1\| + \frac{1}{8}\sum_{j=2}^{4}\|\psi_j\rangle\langle\psi_j\|$	4.55
ρ_{27}	$\frac{7}{16}\|\psi_1\rangle\langle\psi_1\| + \frac{3}{16}\sum_{j=2}^{4}\|\psi_j\rangle\langle\psi_j\|$	4.53
ρ_{28}	$\frac{1}{4}\sum_{j=1}^{4}\|\psi_j\rangle\langle\psi_j\|$	4.50
Average value		4.51

TABLE IV: **Experimental results for Σ, defined in (1), for 28 quantum states.** Notation: $|A\rangle = \frac{|H\rangle+|V\rangle}{\sqrt{2}}$, $|D\rangle = \frac{|H\rangle-|V\rangle}{\sqrt{2}}$, $|h\rangle = \frac{|+2\rangle+|-2\rangle}{\sqrt{2}}$, $|v\rangle = \frac{|+2\rangle-|-2\rangle}{\sqrt{2}}$.

mechanics. *Rev. Mod. Phys.* **38**, 447–452 (1966).

[4] Kochen, S. & Specker, E. P. The problem of hidden variables in quantum mechanics. *J. Math. Mech.* **17**, 59–87 (1967).

[5] Bell, J. S. On the Einstein Podolsky Rosen paradox. *Physics* **1**, 195–200 (1964).

[6] Peres, A. *Quantum Theory: Concepts and Methods* (Kluwer, 1995), 114.

[7] Pavičić, M., Merlet, J.-P., McKay, B. D. & Megill, N. D. Kochen-Specker vectors. *J. Phys. A* **38**, 1577-1592 (2005).

[8] Arends, F., Ouaknine, J. & Wampler, C. W. in *Graph-Theoretic Concepts in Computer Science* (ed. Kolman, P. & Kratochvíl, J.) (Springer, 2011), 23–34.

[9] Cabello, A. How many questions do you need to prove that unasked questions have no answers? *Int. J. Quant. Inf.* **4**, 55–61 (2006).

[10] Cabello, A., Estebaranz, J. M. & García-Alcaine, G. Bell-Kochen-Specker theorem: A proof with 18 vectors. *Phys. Lett. A* **212**, 183–187 (1996).

[11] Peres, A. What's wrong with these observables? *Found. Phys.* **33**, 1543–1547 (2003).

[12] Peres, A. Incompatible results of quantum measurements. *Phys. Lett. A* **151**, 107–108 (1990).

[13] Mermin, N. D. Simple unified form for the major no-hidden-variables theorems. *Phys. Rev. Lett.* **65**, 3373-3376 (1990).

[14] Peres, A. Two simple proofs of the Kochen-Specker theorem. *J. Phys. A* **24**, L175–L178 (1991).

[15] Kernaghan, M. & Peres, A. Kochen-Specker theorem for eight-dimensional space. *Phys. Lett. A* **198**, 1–5 (1995).

[16] Aspect, A., Dalibard, J. & Roger, G. Experimental test of Bell's inequalities using time-varying analyzers. *Phys. Rev. Lett.* **49**, 1804–1807 (1982).

[17] Tittel, W., Brendel, J., Zbinden, H. & Gisin, N. Violation of Bell inequalities by photons more than 10 km apart. *Phys. Rev. Lett.* **81**, 3563–3566 (1998).

[18] Weihs, G., Jennewein, T., Simon, C., Weinfurter, H. & Zeilinger A. Violation of Bell's inequality under strict Einstein locality conditions. *Phys. Rev. Lett.* **81**, 5039–5043 (1998).

[19] Rowe, M. A., Kielpinski, D., Meyer, V., Sackett, C. A., Itano, W. M., Monroe, C. & Wineland, D. J. Experimental violation of a Bell's inequality with efficient detection. *Nature* **409**, 791–794 (2001).

[20] Ekert, A. K. Quantum cryptography based on Bell's the-

orem. *Phys. Rev. Lett.* **67**, 661–663 (1991).

[21] Brukner, Č., Żukowski, M., Pan, J.-W. & Zeilinger, A. Bell's inequalities and quantum communication complexity. *Phys. Rev. Lett.* **92**, 127901 (2004).

[22] Pironio, S., Acín, A., Massar, S., Boyer de la Giroday, A., Matsukevich, D. N., Maunz, P., Olmschenk, S., Hayes, D., Luo, L., Manning, T. A. & Monroe, C. Random numbers certified by Bell's theorem. *Nature* **464**, 1021–1024 (2010).

[23] Nagali, E., D'Ambrosio, V., Sciarrino, F. & Cabello, A. Experimental observation of impossible-to-beat quantum advantage on a hybrid photonic system. *Phys. Rev. Lett.* **108**, 090501 (2012).

[24] Gershenfeld, N. A. & Chuang, I. L. Bulk spin-resonance quantum computation. *Science* **275**, 350–356 (1997).

[25] Cory, D. G., Fahmy, A. F. & Havel, T. F. Ensemble quantum computing by NMR spectroscopy. *PNAS* **94**, 1634–1639 (1997).

[26] Nagali, E., Sansoni, L., Marrucci, L., Santamato, E. & Sciarrino, F. Experimental generation and characterization of single-photon hybrid ququarts based on polarization and orbital angular momentum encoding. *Phys. Rev. A* **81**, 052317 (2010).

[27] Marrucci, L., Karimi, E., Slussarenko, S., Piccirillo, B., Santamato, E., Nagali, E. & Sciarrino, F. Spin-to-orbital conversion of the angular momentum of light and its classical and quantum applications. *J. Opt.* **13**, 064001 (2011).

[28] Nagali, E., Sciarrino, F., De Martini, F., Marrucci, L., Piccirillo, B., Karimi, E. & Santamato, E. Quantum information transfer from spin to orbital angular momentum of photons. *Phys. Rev. Lett.* **103**, 013601 (2009).

[29] Nagali, E., Sciarrino, F., De Martini, F., Piccirillo, B., Karimi, E., Marrucci, L. & Santamato, E. Polarization control of single photon quantum orbital angular momentum states. *Opt. Express* **17**, 18745–18759 (2009).

[30] Piccirillo, B., D'Ambrosio, V., Slussarenko, S., Marrucci, L., & Santamato, E. Photon spin-to-orbital angular momentum conversion via an electrically tunable q-plate. *Appl. Phys. Lett.* **97**, 241104 (2010).

[31] D'Ambrosio, V., Nagali, E., Monken, C. H., Slussarenko, S., Marrucci, L. & Sciarrino, F. Deterministic qubit transfer between orbital and spin angular momentum of single photons. *Opt. Lett.* **37**, 172–174 (2012).

[32] Michler, M., Weinfurter, H. & Żukowski, M. Experiments towards falsification of noncontextual hidden variable theories. *Phys. Rev. Lett.* **84**, 5457–5461 (2000).

[33] Bartosik, H., Klepp, J., Schmitzer, C., Sponar, S., Cabello, A., Rauch, H. & Hasegawa, Y. Experimental test of quantum contextuality in neutron interferometry. *Phys. Rev. Lett.* **103**, 040403 (2009).

[34] Łapkiewicz, R., Li, P., Schaeff, C., Langford, N., Ramelow, S., Wiesniak, M. & Zeilinger, A. Most basic experimental falsification of non-contextuality. *Nature* **474**, 490–493 (2011).

[35] Amselem, E., Danielsen, L. E., López-Tarrida, A. J., Portillo, J. R., Bourennane, M. & Cabello, A. Experimental fully contextual correlations. *Phys. Rev. Lett.* **108**, 200405 (2012).

[36] Cabello, A. Experimentally testable state-independent quantum contextuality. *Phys. Rev. Lett.* **101**, 210401 (2008).

[37] Kirchmair, G., Zähringer, F., Gerritsma, R., Kleinmann, M. Gühne, O., Cabello, A., Blatt, R. & Roos, C. F. State-independent experimental test of quantum contextuality. *Nature* **460**, 494–497 (2009).

[38] Amselem, E., Rådmark, M., Bourennane, M. & Cabello, A. State-independent quantum contextuality with single photons. *Phys. Rev. Lett.* **103**, 160405 (2009).

[39] Moussa, O., Ryan, C. A., Cory, D. G. & Laflamme, R. Testing contextuality on quantum ensembles with one clean qubit. *Phys. Rev. Lett.* **104**, 160501 (2010).

[40] Svozil, K. In *Physics and Computation 2010* (ed. Guerra, H.) (University of Azores, Portugal, 2010), 235–249.

[41] Cabello, A., D'Ambrosio, V., Nagali, E. & Sciarrino, F. Hybrid ququart-encoded quantum cryptography protected by Kochen-Specker contextuality. *Phys. Rev. A* **84**, 030302(R) (2011).

[42] Gühne, O. *et al.* Witnessing the quantum dimension with contextuality. E-print arXiv:1209. . .

[43] Anders, J. & Browne, D. E. Computational power of correlations. *Phys. Rev. Lett.* **102**, 050502 (2009).

[44] Politi, A., Cryan, M. J., Rarity, J. G., Yu, S. & O'Brien, J. L. Silica-on-silicon waveguide quantum circuits. *Science* **320**, 646–649 (2008).

[45] Peruzzo, A., Lobino, M., Matthews, J. C. F., Matsuda, N., Politi, A., Poulios, K., Zhou, X.-Q., Lahini, Y., Ismail, N., Worhoff, K., Bromberg, Y., Silberberg, Y. Thompson, M. G. & O'Brien, J. L. Quantum walks of correlated photons. *Science* **329**, 1500–1503 (2010).

[46] Sansoni, L., Sciarrino, F., Vallone, G., Mataloni, P., Crespi, A., Ramponi, R. & Osellame, R. Polarization entangled state measurement on a chip. *Phys. Rev. Lett.* **105**, 200503 (2010).

[47] Sansoni, L., Sciarrino, F., Vallone, G., Mataloni, P., Crespi, A., Ramponi, R. & Osellame, R. Two-particle bosonic-fermionic quantum walk via integrated photonics. *Phys. Rev. Lett.* **108**, 010502 (2012).

[48] Cabello, A., Severini, S. & Winter, A. (Non-)Contextuality of physical theories as an axiom. E-print arXiv:1010.2163.

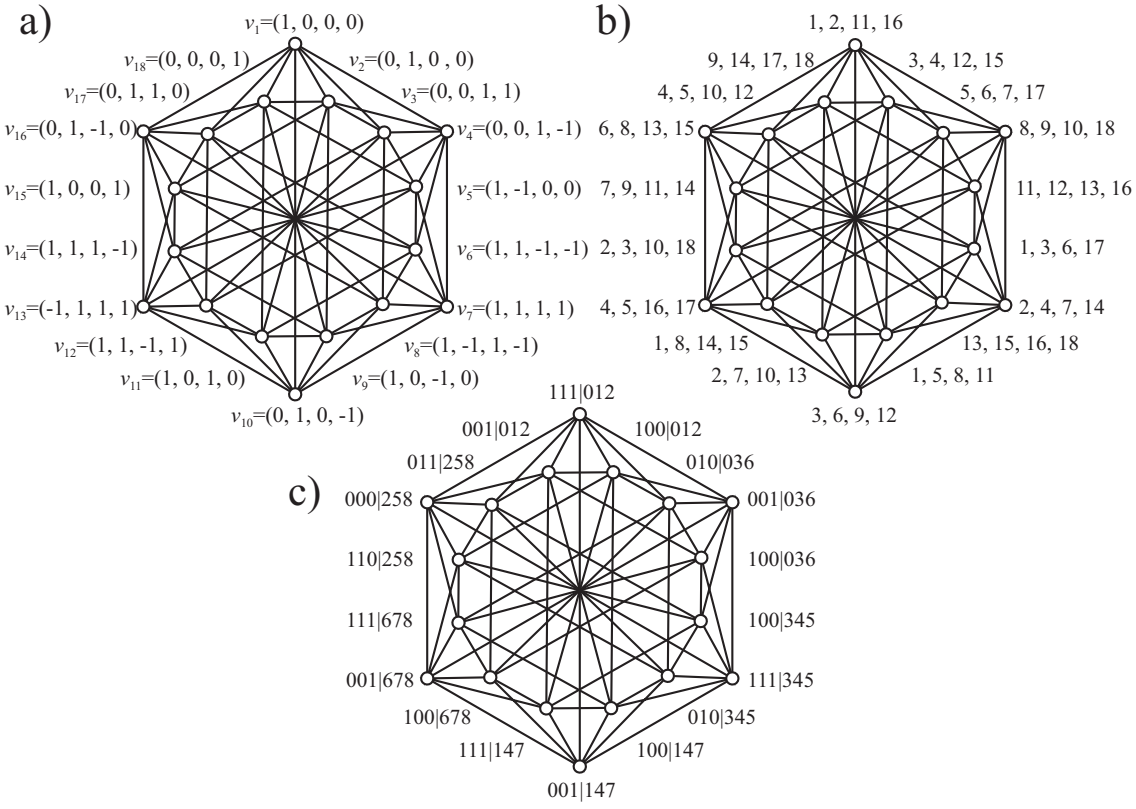

FIG. 1: **a) The 18-test KS set.** Each vertex represents a yes-no test (associated in QM to a projector $\Pi_i = |v_i\rangle\langle v_i|$, where $\langle v_i|$ are the unit vectors displayed in the figure; normalization factors are omitted to simplify the notation), and adjacent vertices correspond to exclusive tests (i.e., they cannot both have the answer yes on the same system; in QM they are associated to orthogonal projectors). This vector representation is the one adopted in our experiments. **b) Optimal strategy for the task described in the text using classical resources.** The system is a ball which can be placed in one out of 18 boxes, and "1, 2, 11, 16" denotes the following yes-no test: "Is the ball in box 1 or in box 2 or in box 11 or in box 16?". The set of classical tests in b) results in the maximum probability of obtaining yes using classical resources (see Supplementary information). **c) Propositions tested in the non-contextuality inequality (5) used to obtain state-independent maximally contextual quantum correlations.** Each vertex represents a proposition $abc|xyz$, denoting "The result of measuring x is a, the result of measuring y is b, and the result of measuring z is c". When the measurements are those in (4), then each of these sequences of measurements and results projects any initial state onto the corresponding state in a).

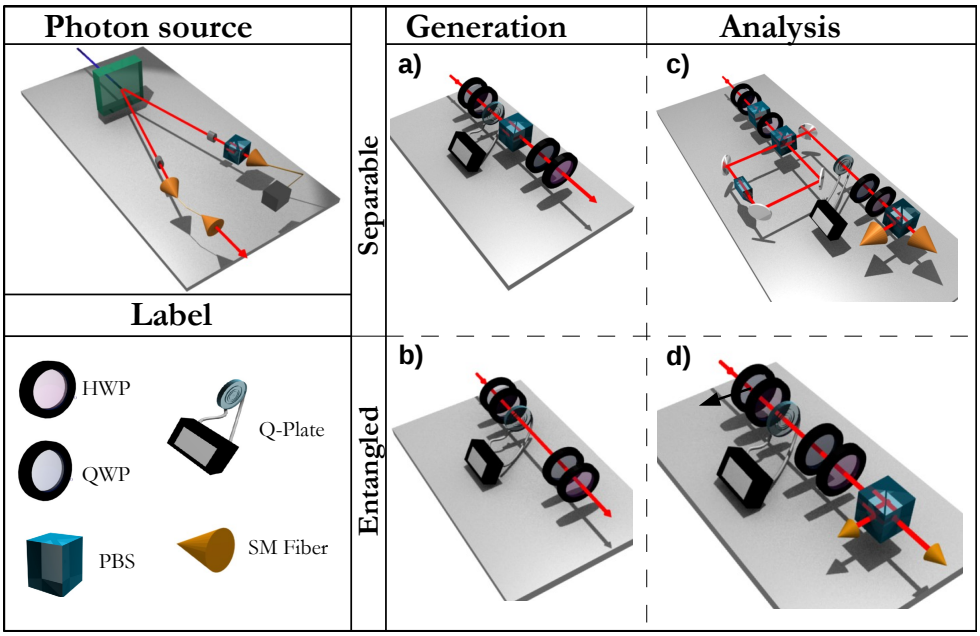

FIG. 2: **Experimental setup for the measurement of the probabilities $P(\Pi_i = 1)$ on different polarization-OAM states.** In the upper left corner is represented the single photon source. The four schemes we used for the experiment are presented in the right part of the figure. Each state is prepared by one of the two setups of the Generation column: Setup a) for separable states (quantum transferrer $\pi \to o_2$ [29]) and setup b) for entangled ones (an "entangler" based on a QP and waveplates). The Analysis column shows the setups for the projection onto the desired states. Setup c) for separable states, a deterministic transferrer $o_2 \to \pi$, and setup d) for entangled states, where a QP is needed to have a deterministic detection.

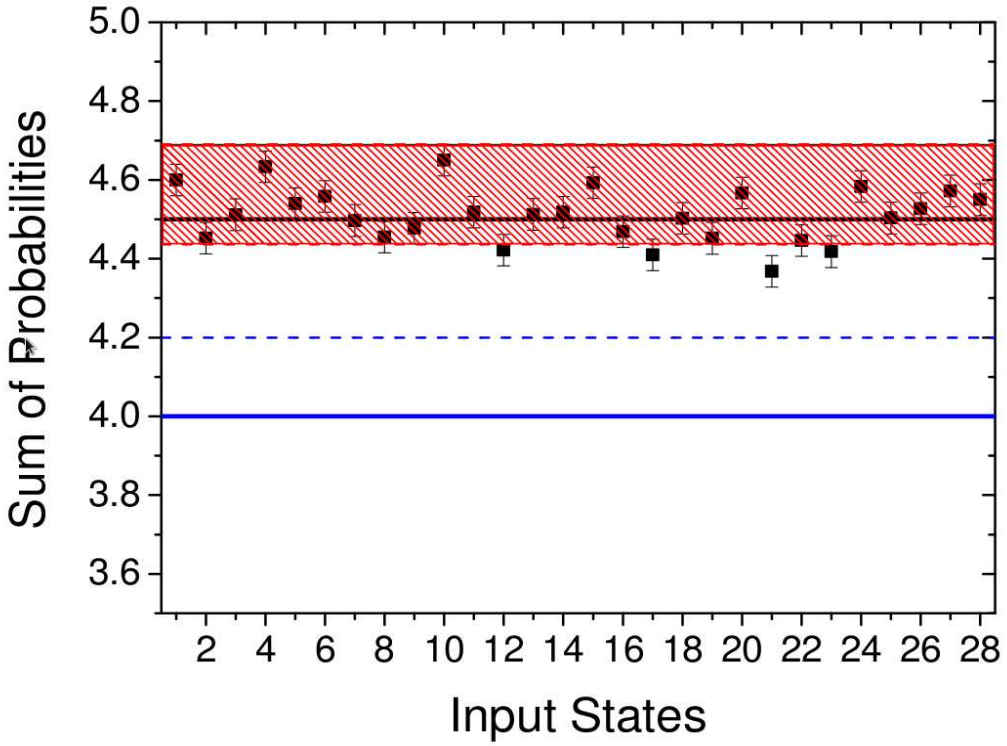

FIG. 3: **Experimental results for Σ for 28 quantum states.** The solid (dashed) blue line refers to the (corrected) classical upper bound for Σ. The red area represents the range $[\Sigma_{min}, \Sigma_{max}]$ in which we theoretically expect to find all experimental values of Σ. The first 18 states correspond to the ones in Fig. 1 a). States 19–28 are defined in Table I.

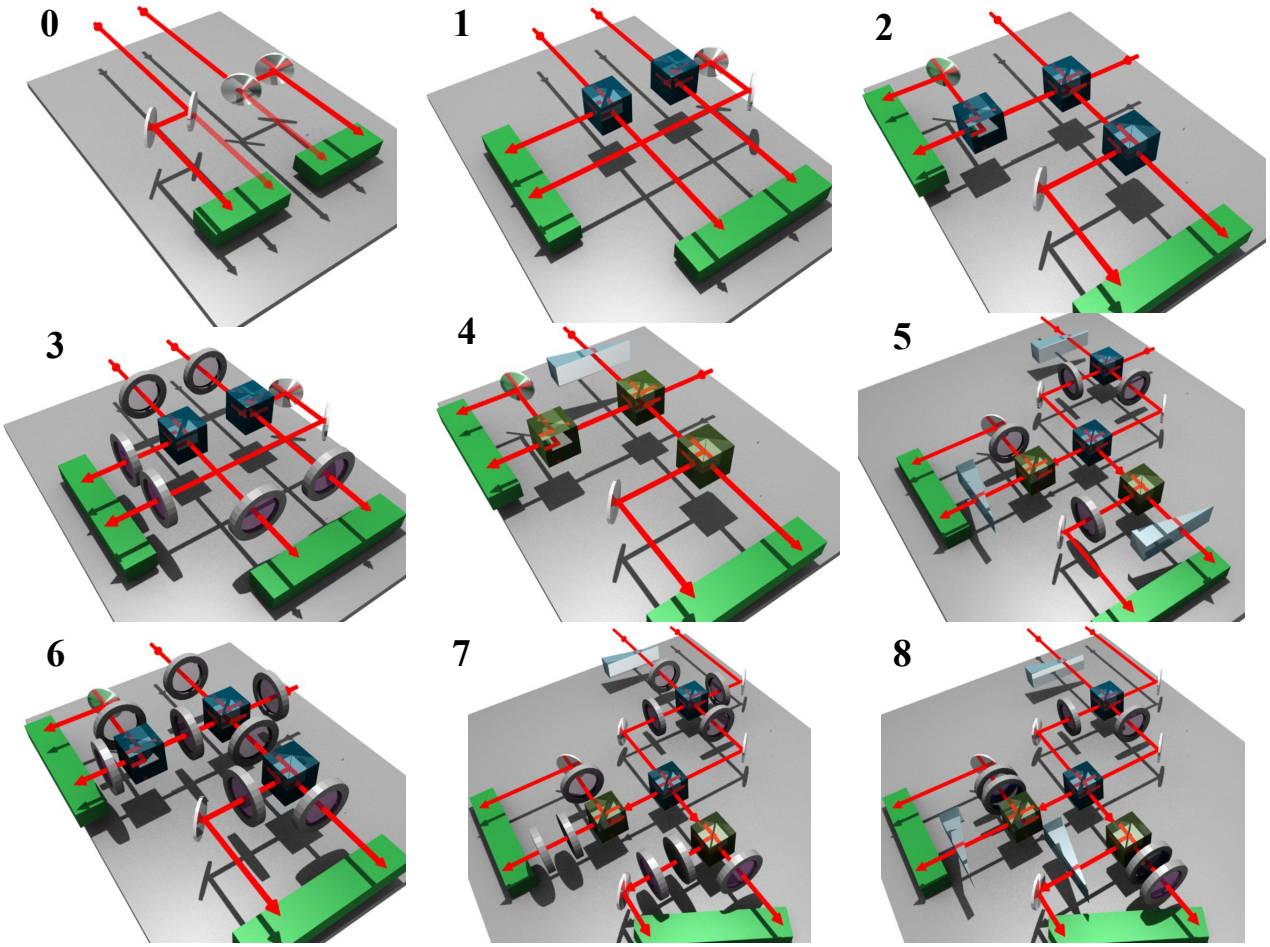

FIG. 4: **Experimental setups for the observables in (4).** For the measurement of observable 0, it is only necessary to distinguish between the paths r and t. An additional beam splitter is needed for observable 1. The measurements of observables 1 and 3 are standard polarization measurements using PBSs and HWPs. Oservables 2, 5, and 8 are Bell state measurements, and so are the measurements of 6 and 7, but then the Bell measurement is preceded by a rotation of the polarization to guarantee compatibility with observable 8. To measure the probabilities appearing in inequality (5), these measurement devices are arranged in a cascaded way [35, 38].

Probabilities		**Probabilities**		**Probabilities**	
$p_{i,j}$	Value	$p_{j,i}$	Value	$p_{i,j}$	Value
$p_{1,2}$	0.02	$p_{7,4}$	0.02	$p_{13,4}$	0.01
$p_{1,3}$	0	$p_{7,5}$	0.02	$p_{13,10}$	0.002
$p_{1,4}$	0	$p_{7,6}$	0	$p_{13,11}$	0.006
$p_{1,10}$	0.008	$p_{7,8}$	0.04	$p_{13,12}$	0.006
$p_{1,16}$	0.02	$p_{7,9}$	0	$p_{13,14}$	0.064
$p_{1,17}$	0.006	$p_{7,10}$	0	$p_{13,15}$	0.032
$p_{1,18}$	0	$p_{7,16}$	0.003	$p_{13,16}$	0.08
$p_{2,1}$	0.003	$p_{8,3}$	0.017	$p_{14,3}$	0.035
$p_{2,3}$	0	$p_{8,6}$	0	$p_{14,5}$	0.018
$p_{2,4}$	0	$p_{8,7}$	0.035	$p_{14,9}$	0.009
$p_{2,9}$	0	$p_{8,7}$	0	$p_{14,12}$	0.005
$p_{2,11}$	0.01	$p_{8,10}$	0	$p_{14,13}$	0.004
$p_{2,15}$	0.007	$p_{8,15}$	0.03	$p_{14,15}$	0.02
$p_{2,18}$	0	$p_{8,17}$	0	$p_{14,16}$	0.012
$p_{3,1}$	0	$p_{9,2}$	0.014	$p_{15,2}$	0.029
$p_{3,2}$	0	$p_{9,7}$	0	$p_{15,6}$	0.01
$p_{3,4}$	0.04	$p_{9,8}$	0	$p_{15,8}$	0.03
$p_{3,5}$	0	$p_{9,10}$	0.034	$p_{15,13}$	0.02
$p_{3,8}$	0.015	$p_{9,11}$	0	$p_{15,14}$	0.01
$p_{3,12}$	0.003	$p_{9,14}$	0.013	$p_{15,16}$	0.01
$p_{3,14}$	0.02	$p_{9,18}$	0.01	$p_{15,17}$	0.01
$p_{4,1}$	0	$p_{10,1}$	0	$p_{16,1}$	0.01
$p_{4,2}$	0	$p_{10,7}$	0	$p_{16,7}$	0.017
$p_{4,3}$	0.042	$p_{10,8}$	0	$p_{16,13}$	0.01
$p_{4,5}$	0	$p_{10,9}$	0.009	$p_{16,14}$	0.06
$p_{4,6}$	0.02	$p_{10,11}$	0	$p_{16,15}$	0.005
$p_{4,7}$	0.03	$p_{10,12}$	0.032	$p_{16,17}$	0.03
$p_{4,13}$	0	$p_{10,13}$	0.053	$p_{16,18}$	0.02
$p_{5,3}$	0	$p_{11,2}$	0.01	$p_{17,1}$	0.007
$p_{5,4}$	0	$p_{11,6}$	0	$p_{17,6}$	0.005
$p_{5,6}$	0.02	$p_{11,9}$	0	$p_{17,8}$	0.02
$p_{5,7}$	0.02	$p_{11,10}$	0	$p_{17,12}$	0.022
$p_{5,12}$	0.02	$p_{11,12}$	0.006	$p_{17,15}$	0.04
$p_{5,14}$	0.006	$p_{11,13}$	0.003	$p_{17,16}$	0.03
$p_{5,18}$	0	$p_{11,18}$	0.01	$p_{17,18}$	0.03
$p_{6,4}$	0.01	$p_{12,3}$	0.009	$p_{18,1}$	0
$p_{6,5}$	0.02	$p_{12,5}$	0.028	$p_{18,2}$	0
$p_{6,7}$	0	$p_{12,10}$	0.033	$p_{18,5}$	0
$p_{6,8}$	0	$p_{12,11}$	0.017	$p_{18,9}$	0
$p_{6,11}$	0	$p_{12,13}$	0.031	$p_{18,11}$	0.001
$p_{6,15}$	0.04	$p_{12,14}$	0	$p_{18,16}$	0.016
$p_{6,17}$	0.09	$p_{12,17}$	0.069	$p_{18,17}$	0.038

TABLE V: **Test of the exclusive disjunction relations.** Experimental values for the probabilities $P_{|v_j\rangle}(\Pi_i = 1) = p_{i,j}$ used for the demonstration of the exclusive disjunction relations between the KS tests. Each pair $\{i, j\}$ corresponds to an edge in the graph in Fig. 1 a).

States	$P(001\|012)$	$P(111\|012)$	$P(100\|012)$	$P(010\|036)$	$P(001\|036)$	$P(100\|036)$
v_1	0.00469 ± 0.00003	0.96943 ± 0.00008	0.00235 ± 0.00002	0.00688 ± 0.00003	0.00246 ± 0.00002	0.46080 ± 0.00039
v_2	0.00816 ± 0.00006	0.00616 ± 0.00005	0.95422 ± 0.00015	0.00831 ± 0.00005	0.00331 ± 0.00003	0.46099 ± 0.00190
v_7	0.25364 ± 0.00048	0.29421 ± 0.00057	0.24430 ± 0.00047	0.40141 ± 0.00013	0.06211 ± 0.00007	0.09906 ± 0.00007
v_{11}	0.01102 ± 0.00007	0.59332 ± 0.00195	0.00507 ± 0.00004	0.23417 ± 0.00032	0.23857 ± 0.00036	0.23913 ± 0.00029
v_{15}	0.47407 ± 0.00034	0.51573 ± 0.00034	0.00079 ± 0.00001	0.17226 ± 0.00014	0.28003 ± 0.00020	0.24091 ± 0.00021
v_{16}	0.00864 ± 0.00005	0.00579 ± 0.00005	0.50176 ± 0.00131	0.23686 ± 0.00071	0.23889 ± 0.00077	0.24422 ± 0.00075
v_{17}	0.01085 ± 0.00007	0.01010 ± 0.00007	0.49884 ± 0.00173	0.23263 ± 0.00063	0.23713 ± 0.00066	0.24524 ± 0.00063
v_{18}	0.95668 ± 0.00062	0.00303 ± 0.00006	0.00477 ± 0.00008	0.41078 ± 0.00086	0.57672 ± 0.00087	0.00077 ± 0.00001
v_{19}	0.02200 ± 0.00017	0.01389 ± 0.00013	0.00482 ± 0.00006	0.48524 ± 0.00194	0.49788 ± 0.00193	0.00157 ± 0.00002
v_{20}	0.01466 ± 0.00008	0.47650 ± 0.00068	0.46002 ± 0.00068	0.00974 ± 0.00004	0.00269 ± 0.00002	0.18468 ± 0.00044
v_{24}	0.47056 ± 0.00100	0.50962 ± 0.00100	0.00139 ± 0.00001	0.23378 ± 0.00074	0.28746 ± 0.00086	0.23480 ± 0.00077
ρ_{25}	0.45592 ± 0.01628	0.49575 ± 0.01645	0.02004 ± 0.00694	0.18569 ± 0.00228	0.27469 ± 0.00246	0.24079 ± 0.00142
ρ_{26}	0.42127 ± 0.02612	0.45821 ± 0.02656	0.05688 ± 0.01134	0.19367 ± 0.00264	0.27209 ± 0.00290	0.24065 ± 0.00164
ρ_{27}	0.38695 ± 0.03270	0.42054 ± 0.03347	0.09327 ± 0.01447	0.20662 ± 0.00274	0.26551 ± 0.00335	0.24091 ± 0.00178
ρ_{28}	0.37036 ± 0.03452	0.40131 ± 0.03542	0.11119 ± 0.01547	0.21979 ± 0.00252	0.26237 ± 0.00339	0.24033 ± 0.00166

TABLE VI: **Experimental values of 6 out of the 18 probabilities needed to test the violation of the non-contextuality inequality (5), for 15 states.** For the other 12 probabilities, see Tables VII and VIII. These experimental values lead to the values of ξ reported in Table II.

States	$P(100\|345)$	$P(111\|345)$	$P(010\|345)$	$P(100\|147)$	$P(001\|147)$	$P(111\|147)$
v_1	0.26452 ± 0.00024	0.20060 ± 0.00020	0.27066 ± 0.00026	0.53399 ± 0.00027	0.01821 ± 0.00007	0.38350 ± 0.00025
v_2	0.22402 ± 0.00017	0.21884 ± 0.00018	0.29808 ± 0.00022	0.02381 ± 0.00004	0.39155 ± 0.00020	0.02196 ± 0.00004
v_7	0.00447 ± 0.00002	0.91502 ± 0.00028	0.01106 ± 0.00003	0.00967 ± 0.00010	0.02254 ± 0.00013	0.47878 ± 0.00021
v_{11}	0.02834 ± 0.00012	0.47805 ± 0.00028	0.44096 ± 0.00028	0.02304 ± 0.00023	0.08027 ± 0.00034	0.84749 ± 0.00041
v_{15}	0.00139 ± 0.00002	0.47787 ± 0.00014	0.00158 ± 0.00002	0.24296 ± 0.00051	0.23698 ± 0.00040	0.25704 ± 0.00052
v_{16}	0.39052 ± 0.00020	0.01284 ± 0.00007	0.53917 ± 0.00020	0.21978 ± 0.00023	0.27539 ± 0.00036	0.19372 ± 0.00024
v_{17}	0.01329 ± 0.00007	0.45783 ± 0.00021	0.01498 ± 0.00008	0.22005 ± 0.00015	0.25323 ± 0.00024	0.22106 ± 0.00016
v_{18}	0.28602 ± 0.00016	0.25611 ± 0.00016	0.21268 ± 0.00020	0.03352 ± 0.00014	0.40537 ± 0.00041	0.03545 ± 0.00012
v_{19}	0.22260 ± 0.00018	0.27739 ± 0.00020	0.24072 ± 0.00018	0.50666 ± 0.00029	0.01810 ± 0.00005	0.41785 ± 0.00028
v_{20}	0.49902 ± 0.00031	0.43034 ± 0.00028	0.02680 ± 0.00027	0.33736 ± 0.00019	0.14444 ± 0.00014	0.25529 ± 0.00015
v_{24}	0.51553 ± 0.00026	0.00638 ± 0.00008	0.44622 ± 0.00026	0.25113 ± 0.00038	0.16467 ± 0.00040	0.28708 ± 0.00043
ρ_{25}	0.07222 ± 0.02157	0.40495 ± 0.02121	0.07689 ± 0.02201	0.23925 ± 0.00136	0.23636 ± 0.00290	0.25100 ± 0.00204
ρ_{26}	0.12609 ± 0.02610	0.34961 ± 0.02528	0.13397 ± 0.02638	0.23742 ± 0.00156	0.23441 ± 0.00357	0.24837 ± 0.00241
ρ_{27}	0.18242 ± 0.02788	0.29159 ± 0.02634	0.19362 ± 0.02793	0.23597 ± 0.00181	0.22921 ± 0.00445	0.24599 ± 0.00286
ρ_{28}	0.24562 ± 0.02897	0.22560 ± 0.02666	0.26257 ± 0.02892	0.23366 ± 0.00183	0.23354 ± 0.00458	0.23879 ± 0.00297

TABLE VII: **Experimental values of 6 out of the 18 probabilities needed to test the violation of the non-contextuality inequality (5), text for 15 states.** For the other 12 probabilities, see Tables VI and VIII. These experimental values lead to the values of ξ reported in Table II.

States	$P(100\|678)$	$P(001\|678)$	$P(111\|678)$	$P(110\|258)$	$P(000\|258)$	$P(011\|258)$
v_1	0.20429 ± 0.00026	0.20198 ± 0.00036	0.21255 ± 0.00022	0.45072 ± 0.00124	0.00162 ± 0.00001	0.00606 ± 0.00003
v_2	0.21116 ± 0.00019	0.27606 ± 0.00028	0.20309 ± 0.00030	0.00370 ± 0.00002	0.46596 ± 0.00107	0.48961 ± 0.00108
v_7	0.24464 ± 0.00027	0.17138 ± 0.00013	0.24261 ± 0.00026	0.34784 ± 0.00028	0.01168 ± 0.00005	0.56462 ± 0.00036
v_{11}	0.00696 ± 0.00005	0.00827 ± 0.00006	0.45328 ± 0.00044	0.22640 ± 0.00053	0.21397 ± 0.00053	0.31228 ± 0.00073
v_{15}	0.40428 ± 0.00013	0.01273 ± 0.00002	0.00945 ± 0.00003	0.92373 ± 0.00033	0.00439 ± 0.00002	0.00448 ± 0.00002
v_{16}	0.43543 ± 0.00016	0.01655 ± 0.00009	0.00642 ± 0.00002	0.01271 ± 0.00002	0.88871 ± 0.00037	0.02764 ± 0.00009
v_{17}	0.00580 ± 0.00002	0.47776 ± 0.00042	0.39824 ± 0.00050	0.00173 ± 0.00001	0.02191 ± 0.00003	0.87828 ± 0.00031
v_{18}	0.16293 ± 0.00012	0.28624 ± 0.00020	0.17858 ± 0.00032	0.48059 ± 0.00030	0.00743 ± 0.00002	0.00240 ± 0.00001
v_{19}	0.23814 ± 0.00020	0.22213 ± 0.00015	0.21773 ± 0.00018	0.00918 ± 0.00003	0.40457 ± 0.00077	0.53408 ± 0.00078
v_{20}	0.38909 ± 0.00030	0.04651 ± 0.00006	0.40079 ± 0.00032	0.18890 ± 0.00016	0.26179 ± 0.00019	0.28265 ± 0.00021
v_{24}	0.01863 ± 0.00005	0.46692 ± 0.00023	0.32780 ± 0.00026	0.01507 ± 0.00008	0.00529 ± 0.00001	0.00447 ± 0.00001
ρ_{25}	0.34260 ± 0.01553	0.08828 ± 0.01954	0.06934 ± 0.01618	0.70423 ± 0.04253	0.06367 ± 0.02803	0.09191 ± 0.03489
ρ_{26}	0.29852 ± 0.01854	0.14204 ± 0.02265	0.10917 ± 0.01866	0.57473 ± 0.04545	0.13755 ± 0.03791	0.11320 ± 0.03737
ρ_{27}	0.26977 ± 0.01972	0.17678 ± 0.02360	0.13295 ± 0.01927	0.32880 ± 0.04335	0.18683 ± 0.04094	0.22940 ± 0.04564
ρ_{28}	0.22907 ± 0.02072	0.22915 ± 0.02352	0.17698 ± 0.02009	0.21618 ± 0.03903	0.25357 ± 0.04370	0.24670 ± 0.04584

TABLE VIII: **Experimental values of 6 out of the 18 probabilities needed to test the violation of the non-contextuality inequality (5), for 15 states.** For the other 12 probabilities, see Tables VI and VII. These experimental values lead to the values of ξ reported in Table II.

LETTERS
PUBLISHED ONLINE: 10 JUNE 2012 | DOI: 10.1038/NPHYS2334
nature physics

Experimental estimation of the dimension of classical and quantum systems

Martin Hendrych[1], Rodrigo Gallego[1], Michal Mičuda[1,2], Nicolas Brunner[3], Antonio Acín[1,4]* and Juan P. Torres[1,5]*

Experimental observations are usually described using theoretical models that make assumptions about the dimensionality of the system under consideration. However, would it be possible to assess the dimension of a completely unknown system only from the results of measurements performed on it, without any extra assumption? The concept of a dimension witness[1–6] answers this question, as it allows bounding the dimension of an unknown system only from measurement statistics. Here, we report on the experimental demonstration of dimension witnesses in a prepare and measure scenario[6]. We use photon pairs entangled in polarization and orbital angular momentum[7–9] to generate ensembles of classical and quantum states of dimensions up to 4. We then use a dimension witness to certify their dimensionality as well as their quantum nature. Our work opens new avenues in quantum information science, where dimension represents a powerful resource[10–12], especially for device-independent estimation of quantum systems[13–16] and quantum communications[17,18].

Dimensionality is one of the most basic and essential concepts in science, inherent to any theory aiming at explaining and predicting experimental observations. In building up a theoretical model, one makes some general and plausible assumptions about the nature and the behaviour of the system under study. The dimension of this system, that is, the number of relevant and independent degrees of freedom needed to describe it, represents one of these initial assumptions. In general, the failure of a theoretical model in predicting experimental data does not necessarily imply that the assumption on the dimensionality is incorrect, because there might exist a different model assuming the same dimension that is able to reproduce the observed data.

A natural question is whether this approach can be reversed and whether the dimension of an unknown system, classical or quantum, can be estimated experimentally. Clearly, the best one can hope for is to provide lower bounds on this unknown dimension. Indeed, every physical system has potentially an infinite number of degrees of freedom, and one can never exclude that they are all necessary to describe the system in more complex experimental arrangements. The goal, then, is to obtain a lower bound on the dimension of the unknown system from the observed measurement data without making any assumption about the detailed functioning of the devices used in the experiment. Besides its fundamental interest, estimating the dimension of an unknown quantum system is also relevant from the perspective of quantum information science, where the Hilbert space dimension is considered as a resource. For instance, using higher-dimensional Hilbert spaces simplifies quantum logic for quantum computation[10], enables the optimal realization of information-theoretic protocols[11,19,20] and allows for lower detection efficiencies in Bell experiments[21,22]. Moreover, the dimension of quantum systems plays a crucial role in security proofs of standard quantum key distribution schemes that become insecure if the dimension is higher than assumed[12].

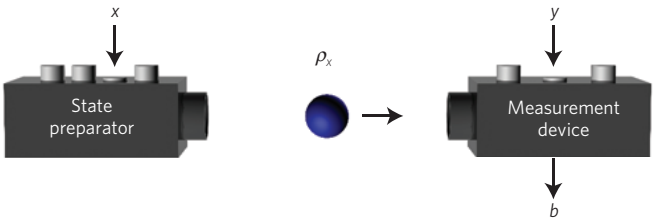

Figure 1 | Sketch of a device-independent test of the dimension of an ensemble of states. Our scenario features two black boxes. First, a state preparator that, on request, prepares the mediating particle in one out of N possible states. Second, a measurement device that performs one out of M possible measurements on the mediating particle.

The concept of a dimension witness allows one to establish lower bounds on the dimension of an unknown system in a device-independent way, that is, only from the collected measurement statistics. It was first introduced for quantum systems in connection with Bell inequalities in ref. 1, and further developed in refs 2, 3,22–26. Other techniques to estimate the dimension have been developed in scenarios involving random access codes[4], or the time evolution of a quantum observable[5].

More recently, a general framework for the study of this question has been proposed in ref. 6. In this approach, dimension witnesses are defined in a prepare and measure scenario where an unknown system is subject to different preparations and measurements. One of the advantages of this approach is its simplicity from an experimental viewpoint when compared with previous proposals. The considered scenario consists of two devices (Fig. 1), the state preparator and the measurement device. These devices are seen as black boxes, as no assumptions are made on their functioning. The state preparator prepares a state on request. The box features N buttons that label the prepared state; when pressing button x, the box emits a state ρ_x, where $x \in \{1,\ldots,N\}$. The prepared state is then sent to the measurement device. The measurement box performs a measurement $y \in \{1,\ldots,M\}$ on the state, delivering outcome $b \in \{1,\ldots,K\}$. The experiment is thus described by the probability distribution $P(b|x,y)$, giving the probability of obtaining outcome

[1]ICFO-Institut de Ciencies Fotoniques, 08860 Castelldefels (Barcelona), Spain, [2]Department of Optics, Palacký University, 17. listopadu 12, 77146 Olomouc, Czech Republic, [3]H.H. Wills Physics Laboratory, University of Bristol, Bristol BS8 1TL, UK, [4] ICREA-Institució Catalana de Recerca i Estudis Avançats, 08010 Barcelona, Spain, [5]Department of Signal Theory and Communications, Universitat Politècnica de Catalunya, 08034 Barcelona, Spain. *e-mail: antonio.acin@icfo.es; juanp.torres@icfo.es.

Table 1 | Classical and quantum bounds for the dimension witness I_4.

	C_2 (bit)	Q_2 (qubit)	C_3 (trit)	Q_3 (qutrit)	C_4 (quart)
I_4	5	6	7	7.97	9

The maximal possible value of I_4 for classical systems of dimension d is denoted C_d, and the maximum possible value for quantum systems of dimension d is denoted Q_d. The witness can be used to discriminate ensembles of classical and quantum states of dimension up to $d=4$. Note that for some values of d we have that $C_d < Q_d$. Thus, if one assumes a bound on the dimension of the system, the witness can be used to certify its quantum nature.

b when measurement y is performed on the prepared state ρ_x. The goal is to estimate the minimal dimension that the ensemble $\{\rho_x\}$ must have to be able to describe the observed statistics. Moreover, for a fixed dimension, we also aim at distinguishing sets of probabilities $P(b|x,y)$ that can be obtained from ensembles of quantum states, but not from ensembles of classical states. This allows one to guarantee the quantum nature of an ensemble of states under the assumption that the dimensionality is bounded. This quantum certification can be exploited for the design of quantum information protocols[17,18].

Formally, a probability distribution $P(b|x,y)$ admits a quantum d-dimensional representation if it can be written in the form

$$P(b|x,y) = \mathrm{tr}(\rho_x O_b^y) \tag{1}$$

for some state ρ_x and measurement operator O_b^y acting on $\mathbb{C}^d$. We then say that $P(b|x,y)$ has a classical d-dimensional representation if any state of the ensemble $\{\rho_x\}$ is a classical state of dimension d, that is, a probability distribution over classical dits (the equivalent in quantum mechanics is that all states in the ensemble act on $\mathbb{C}^d$ and commute pairwise).

A dimension witness for systems of dimension d is defined by a linear combination of the observed probabilities $P(b|x,y)$, defined by a tensor of real coefficients $D_{b,x,y}$, such that

$$\sum_{b,x,y} D_{b,x,y} P(b|x,y) \leq w_d \tag{2}$$

for all probabilities with a d-dimensional representation, whereas the bound w_d can be violated by a set of probabilities whose representation has a dimension strictly larger than d. Here we shall focus on a dimension witness of the form of equation (2) recently introduced in ref. 6, for a scenario consisting of $N=4$ possible preparations and $M=3$ measurements with only two possible outcomes, labelled by $b=\pm 1$:

$$I_4 \equiv E_{11}+E_{12}+E_{13}+E_{21}+E_{22}-E_{23}+E_{31}-E_{32}-E_{41} \tag{3}$$

where $E_{xy} = P(b=+1|x,y) - P(b=-1|x,y)$. The witness I_4 can distinguish ensembles of classical and quantum states of dimensions up to $d=4$. All of the relevant bounds are summarized in Table 1.

To test this witness experimentally, we must generate classical and quantum states of dimension 2 (bits and qubits, respectively), classical and quantum states of dimension 3 (trits and qutrits), and classical states of dimension 4 (quarts). To do so we exploit the angular momentum of photons[7,8], which contains a spin contribution associated with the polarization, and an orbital contribution associated with the spatial shape of the light intensity and its phase. Within the paraxial regime, both contributions can be measured and manipulated independently. The polarization of photons is conveniently represented by a two-dimensional Hilbert space, spanned by two orthogonal polarization states (for example, horizontal and vertical). The spatial degree of freedom of light lives in an infinite-dimensional Hilbert space[27], spanned by paraxial Laguerre–Gaussian modes. Laguerre–Gaussian beams carry a well-defined orbital angular momentum (OAM) of $m\hbar$ (m is an integer) per photon that is associated with their spiral wavefronts[28].

In our experiment, we use both the polarization and the OAM ($m=\pm 1$) of photons to prepare quantum states of dimension up to 4, spanned by the orthogonal vectors $|H,+1\rangle$, $|H,-1\rangle$, $|V,+1\rangle$ and $|V,-1\rangle$, where $|H,\pm 1\rangle$ ($|V,\pm 1\rangle$) denotes a horizontally (vertically) polarized photon with OAM $m=\pm 1$. We first generate, by means of spontaneous parametric down-conversion, pairs of photons (signal and idler) entangled in both polarization and OAM (Fig. 2). The entangled state is of the form $|\Psi^-\rangle_{\mathrm{pol}} \otimes |\Psi^-\rangle_{\mathrm{OAM}}$, where $|\Psi^-\rangle_{\mathrm{pol}} = (1/\sqrt{2})(|H\rangle_s|V\rangle_i - |V\rangle_s|H\rangle_i)$ and $|\Psi^-\rangle_{\mathrm{OAM}} = (1/\sqrt{2})(|m=1\rangle_s|m=-1\rangle_i + |m=-1\rangle_s|m=1\rangle_i)$. By performing a projective measurement on the idler photon, we prepare the signal photon in a well-defined state of polarization and OAM. In particular, we project the idler photon on states of the form $(\cos\theta|H\rangle_i + \sin\theta|V\rangle_i) \otimes |m=\pm 1\rangle_i$, which has the effect of preparing the signal photon in the state $(\sin\theta|H\rangle_s - \cos\theta|V\rangle_s) \otimes |m=\mp 1\rangle_s$. Thus, the combination of the source of entanglement and the measurement of the idler photon represents the state preparator. The prepared state is encoded on the signal photon that is then measured. The signal photon represents the mediating particle between the state preparator and measurement device of Fig. 1.

To implement a continuous transition from quantum to classical states, a polarization-dependent temporal delay τ between the signal and idler photons is introduced. If the temporal delay between the photons exceeds their correlation time, the coherence is lost; that is, the off-diagonal terms vanish for all states in the ensemble (see Supplementary Information).

For the sake of clarity, we list the assumptions made when processing the observed data: the statistical behaviour of $P(b|xy)$, described by equation (1), is the same at every run of the experiment; the detectors used for the preparation and the measurement are uncorrelated; the observer can freely choose the preparation and measurement in each run; the observed statistics provide a fair sample of the total statistics that would have been observed with perfect detectors. All of these assumptions are standard in any estimation scenario. The value of the dimension witnesses is then calculated from the raw data, that is, from all of the observed coincidences between detection at the preparator and at the measuring device, including dark counts. In the experiment we first generate and measure the four qubit states $|\phi_x\rangle$ given in Fig. 2. The first measurement ($y=1$) assigns dichotomic measurement results of $b=+1$ and $b=-1$ to horizontally and vertically polarized photons, respectively. The second measurement ($y=2$) assigns $b=+1$ and $b=-1$ to OAM values of $m=+1$ and $m=-1$, respectively. The third measurement ($y=3$) assigns $b=+1$ and $b=-1$ to photons polarized at $+45°$ and $-45°$, respectively. The expected value of the dimension witness of equation (3) for this combination of states and measurements is $I_4 = 3+2\sqrt{2} \sim 5.83$ (see Supplementary Information). From our experimental data we obtain $I_4 = 5.66 \pm 0.15$. This clearly demonstrates the quantum nature of our two-dimensional system, because classical bits always satisfy $I_4 \leq 5$.

In the above, the delay between signal and idler photons was set to $\tau = 0$. Now we gradually increase this delay to convert a qubit into a classical bit. The measured value of the witness I_4 then drops below 5, as expected (blue triangles in Fig. 3).

Next we generate ensembles of qutrits. The prepared states and the measurements are identical to the previous (qubit) experiment, except that the OAM of state $|\phi_3\rangle$ is now flipped. For $\tau = 0$, we obtain a measured value of the witness of $I_4 = 7.57 \pm 0.13$, certifying the presence of a quantum system of dimension (at least) 3. This value is in good agreement with the theoretical prediction of $I_4 = 5+2\sqrt{2} \sim 7.83$ for this set of states and measurements.

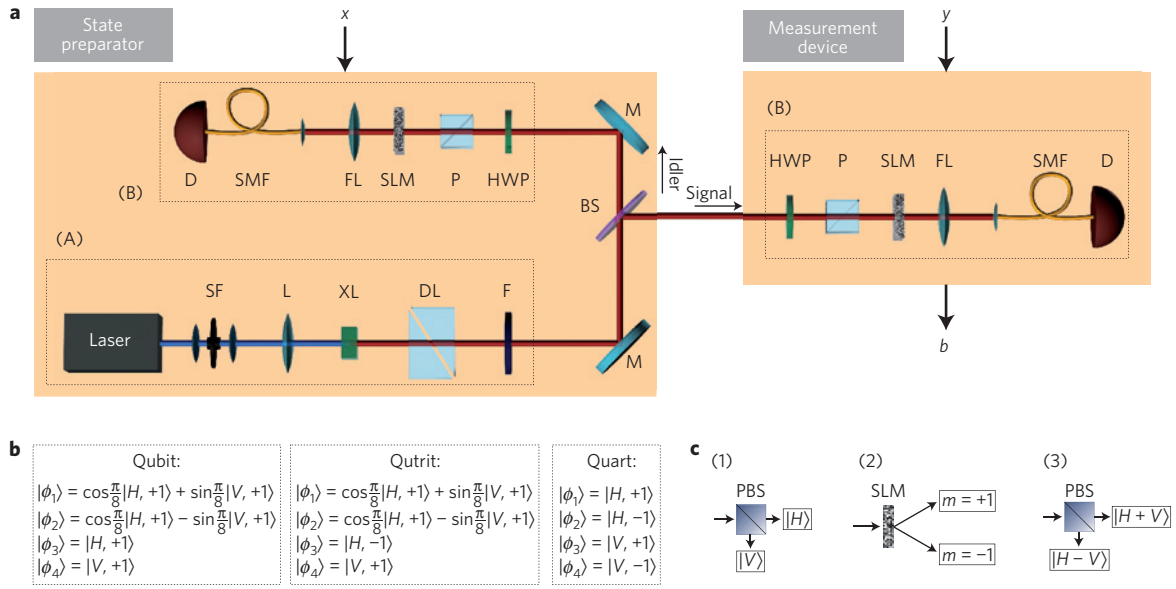

Figure 2 | Experimental set-up. a, The state preparator consists of a source of entangled photons (A), followed by a measurement (B) on one photon of the pair (idler) that prepares its twin photon (signal) in the desired state. The signal photon is then sent to the measurement device. Block (A) is the source of entangled photons. The second harmonic (Inspire Blue, Spectra Physics/Radiantis) at a wavelength of 405 nm of a Ti:sapphire laser in the picosecond regime (Mira, Coherent) is shaped by a spatial filter (SF) and focused into a 1.5-mm-thick crystal of beta-barium borate, where spontaneous parametric down-conversion takes place. The nonlinear crystal (XL) is cut for collinear type-II down-conversion so that the generated photons have orthogonal polarizations. Before splitting the signal and idler photon, a polarization-dependent temporal delay τ is introduced. The delay line (DL) consists of two quartz prisms whose mutual position determines the difference between the propagation times of photons with orthogonal polarizations. Block (B) performs a measurement on the idler photon to prepare the signal photon. It consists of a half-wave plate (HWP), polarizer (P), spatial-light modulator (SLM) and a Fourier-transform lens (FL). The half-wave plate and polarizer project the photon into the desired polarization state. The desired OAM state is selected by the SLM. SLM encodes computer-generated holograms that transform the $m=+1$ state or $m=-1$ state into the fundamental Laguerre–Gaussian state LG_{00} (ref. 7) that is coupled into a single-mode fibre (SMF). The measurement device uses an identical block (B) to measure the signal photon. M: mirrors; L: lenses; BS: beam splitter, F: interference filter; D: single-photon counting modules. **b**, Ensembles of quantum states $|\phi_x\rangle$ ($x=1\ldots4$) prepared in the experiment. **c**, Measurements performed at the measurement device for qubits and qutrits. In the case of quarts, the three measurements are constructed by combining (1) and (2).

Now, increasing again delay τ between the photons, the value of the witness drops below 7. In a certain range of delays, the value of I_4 remains above the qubit bound of 6, testifying that at least three dimensions are present (red circles of Fig. 3). In the limit of large delays, the values of the witness are still larger than the bound of $I_4=5$ for bits, but below the bound for qubits. This is because the curve was measured with a set a measurements optimized for the qutrit/trit discrimination. This set of measurements is not optimum for the trit/qubit discrimination.

Finally, we prepare classical four-dimensional systems, that is, quarts. Now the first measurement ($y=1$) assigns the outcome $b=-1$ to vertically polarized photons with OAM $m=-1$, and the outcome $b=+1$ to all of the other orthogonal states. The second measurement ($y=2$) assigns $b=+1$ and $b=-1$ to horizontally and vertically polarized photons, respectively. The third measurement ($y=3$) assigns $b=+1$ and $b=-1$ to OAM of $m=+1$ and $m=-1$, respectively. In this case, the expected value of the witness is $I_4=9$, which corresponds to the algebraic maximum. Experimentally, we measure $I_4=8.57\pm0.06$, which violates the qutrit bound of $I_4=7.97$ by more than 10 standard deviations. In this case, the values of the witness are independent of the temporal delay τ. This is because the state is here classical (a statistical mixture of orthogonal quantum states) and no superposition is present (green diamonds in Fig. 3).

We have demonstrated how the concept of dimensionality, which is fundamental in science, can be experimentally tested. Using dimension witnesses, we have bounded the dimension of classical and quantum systems only from measurement statistics, without any assumption on the internal working of the devices

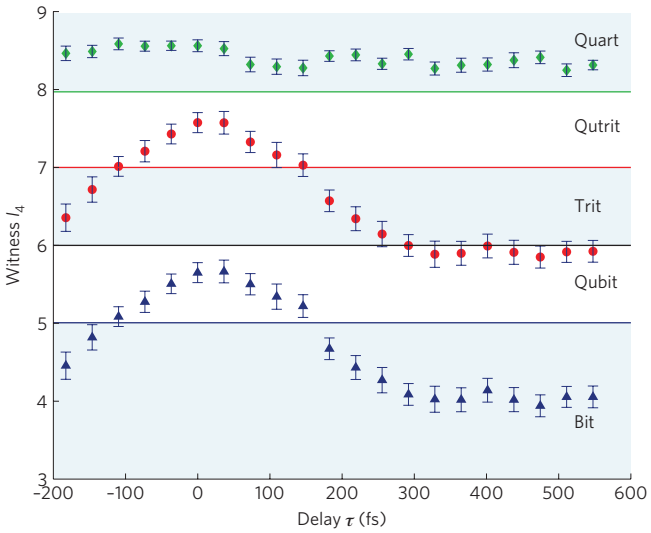

Figure 3 | Dimension witness I_4 for qubit (blue triangles), qutrit (red circles) and quart (green diamonds) states as a function of temporal delay τ. For delays $\tau > 255$ fs, coherence is lost and quantum superpositions turn into statistical mixtures, that is, classical states. The maximum observed violations for qubit, qutrit and quart states are 5.66 ± 0.15, 7.57 ± 0.13 and 8.57 ± 0.06, respectively. These values are close to the corresponding theoretical bounds, given in Table 1, which are represented here by the horizontal lines. The error bars plot standard deviations on the value of the witness calculated from the measured data using error propagation rules.

used in the experiment. Dimension witnesses represent an example of a device-independent estimation technique, in which relevant information about an unknown system is obtained solely from the measurement data. Device-independent techniques[13–16] provide an alternative approach to existing quantum estimation techniques, such as quantum tomography or entanglement witnesses, which crucially rely on assumptions that may be questionable in complex set-ups, for example, its Hilbert space dimension. Our work demonstrates how the device-independent approach can be employed to experimentally estimate the dimension of an unknown system.

Received 4 March 2012; accepted 3 May 2012; published online 10 June 2012

References

1. Brunner, N., Pironio, S., Acín, A., Gisin, N., Méthot, A. & Scarani, V. Testing the dimension of Hilbert spaces. *Phys. Rev. Lett.* **100,** 210503 (2008).
2. Pál, K. & Vértesi, T. Efficiency of higher-dimensional Hilbert spaces for the violation of Bell inequalities. *Phys. Rev. A* **77,** 042105 (2008).
3. Pérez-García, D., Wolf, M. M., Palazuelos, C., Villanueva, I. & Junge, M. Unbounded violation of tripartite Bell inequalities. *Commun. Math. Phys.* **279,** 455–486 (2008).
4. Wehner, S., Christandl, M. & Doherty, A. C. Lower bound on the dimension of a quantum system given measured data. *Phys. Rev. A* **78,** 062112 (2008).
5. Wolf, M. M. & Pérez-García, D. Assessing quantum dimensionality from observable dynamics. *Phys. Rev. Lett.* **102,** 190504 (2009).
6. Gallego, R., Brunner, N., Hadley, C. & Acín, A. Device-independent tests of classical and quantum dimensions. *Phys. Rev. Lett.* **105,** 230501 (2010).
7. Molina-Terriza, G., Torres, J. P. & Torner, L. Twisted photons. *Nature Phys.* **3,** 305–310 (2007).
8. Mair, A., Vaziri, A., Weihs, G. & Zeilinger, A. Entanglement of the orbital angular momentum states of photons. *Nature* **412,** 313–316 (2001).
9. Dada, A. C., Leach, J., Buller, G. S., Padgett, M. J. & Andersson, E. Experimental high-dimensional two-photon entanglement and violations of generalized Bell inequalities. *Nature Phys.* **7,** 677–680 (2011).
10. Lanyon, B. *et al.* Simplifying quantum logic using higher-dimensional Hilbert spaces. *Nature Phys.* **5,** 134–140 (2009).
11. Spekkens, R. W. & Rudolph, T. Degrees of concealment and bindingness in quantum bit commitment protocols. *Phys. Rev. A* **65,** 012310 (2001).
12. Acín, A., Gisin, N. & Masanes, Ll. From Bell's theorem to secure quantum key distribution. *Phys. Rev. Lett.* **97,** 120405 (2006).
13. Mayers, D. & Yao, A. Self testing quantum apparatus. *Quant. Inf. Comp.* **4,** 273–286 (2004).
14. Bardyn, C.-E., Liew, T. C. H., Massar, S., McKague, M. & Scarani, V. Device-independent state estimation based on Bell's inequalities. *Phys. Rev. A* **80,** 062327 (2009).
15. Bancal, J-D., Gisin, N., Liang, Y-C. & Pironio, S. Device-independent witnesses of genuine multipartite entanglement. *Phys. Rev. Lett.* **106,** 250404 (2011).
16. Rabelo, R., Ho, M., Cavalcanti, D., Brunner, N. & Scarani, V. Device-independent certification of entangled measurements. *Phys. Rev. Lett.* **107,** 050502 (2011).
17. Pawlowski, M. & Brunner, N. Semi-device-independent security of one-way quantum key distribution. *Phys. Rev. A* **84,** 010302 (2011).
18. Li, H-W. *et al.* Semi-device-independent random-number expansion without entanglement. *Phys. Rev. A* **84,** 034301 (2011).
19. Langford, N. K. *et al.* Measuring entangled qutrits and their use for quantum bit commitment. *Phys. Rev. Lett.* **93,** 053601 (2004).
20. Molina-Terriza, G., Vaziri, A., Ursin, R. & Zeilinger, A. Experimental Quantum Coin Tossing. *Phys. Rev. Lett.* **94,** 040501 (2005).
21. Massar, S. Nonlocality, closing the detection loophole, and communication complexity. *Phys. Rev. A* **65,** 032121 (2002).
22. Vértesi, T., Pironio, S. & Brunner, N. Closing the detection loophole in bell experiments using qudits. *Phys. Rev. Lett.* **104,** 060401 (2010).
23. Vértesi, T. & Pál, K. Generalized Clauser-Horne-Shimony-Holt inequalities maximally violated by higher-dimensional systems. *Phys. Rev. A* **77,** 042106 (2008).
24. Junge, M., Palazuelos, C., Pérez-García, D., Villanueva, I. & Wolf, M. M. Operator space theory: A natural framework for bell inequalities. *Phys. Rev. Lett.* **104,** 170405 (2010).
25. Briët, J., Buhrman, H. & Toner, B. A generalized Grothendieck inequality and nonlocal correlations that require high entanglement. *Commun. Math. Phys.* **305,** 827–843 (2011).
26. Junge, M. & Palazuelos, C. Large violation of Bell inequalities with low entanglement. *Commun. Math. Phys.* **306,** 695–746 (2011).
27. Molina-Terriza, G., Torres, J. P. & Torner, L. Management of the orbital angular momentum of light: Preparation of photons in multidimensional vector states of angular momentum. *Phys. Rev. Lett.* **88,** 013601 (2002).
28. Allen, L., Beijersbergen, M. W., Spreeuw, R. J. C. & Woerdman, J. P. Orbital angular momentum of light and the transformation of Laguerre–Gaussian laser modes. *Phys. Rev. A* **45,** 8185–8189 (1992).

Acknowledgements

We thank C. Hadley and E. Nagali for contributions in early stages of this work. We acknowledge support from the ERC Starting Grant PERCENT, the EU Projects Q-Essence, QCS and PHORBITECH (FET OPEN grant number 255914), the UK EPSRC, the Project MSM6198959213 of the Czech Ministry of Education, the Spanish projects FIS2010-14830, FIS2010-14831 and Chist-Era DIQIP, an FI Grant of the Generalitat de Catalunya, CatalunyaCaixa, and Fundació Privada Cellex, Barcelona.

Author contributions

R.G., N.B. and A.A. developed the theory, M.H., R.G., N.B., A.A. and J.P.T. designed the experiment, and M.H., M.M. and J.P.T. performed the experiment. All of the authors contributed to the writing of the manuscript.

Additional information

The authors declare no competing financial interests. Supplementary information accompanies this paper on www.nature.com/naturephysics. Reprints and permissions information is available online at www.nature.com/reprints. Correspondence and requests for materials should be addressed to A.A. (theory) and J.P.T. (experiment).